Electronic Supplementary Material (ESI) for Inorganic Chemistry Frontiers.

Supporting information for:

Exceptionally fast formation of stable rigidified cross-bridged complexes formed with Cu(II) isotopes for Molecular Imaging

Tibor Csupász,[a] Norbert Lihi,*[b] Zsuzsa Fekete,[a] Antónia Nagy,[a] Richárd Botár,[a] Viktória Forgács,[c] Dezső Szikra,[c] Nóra Veronika May,[d] Gyula Tircsó[a] and Ferenc Krisztián Kálmán*[a]

[a] *Department of Physical Chemistry,University of Debrecen, H-4032 Debrecen, Egyetem tér 1., Hungar, E-mail: kalman.ferenc@science.unideb.hu.*

[b] *Department of Inorganic and Analytical Chemistry, University of Debrecen, H-4032 Debrecen, Egyetem tér 1., Hungary*

[c] *Division of Nuclear Medicine and Translational Imaging, Department of Medical Imaging, University of Debrecen, H-4032 Debrecen, Egyetem tér 1., Hungary*

[d] *Centre for Structural Science, Research Centre for Natural Sciences, Budapest H-1519, Hungary*

Table of Contents

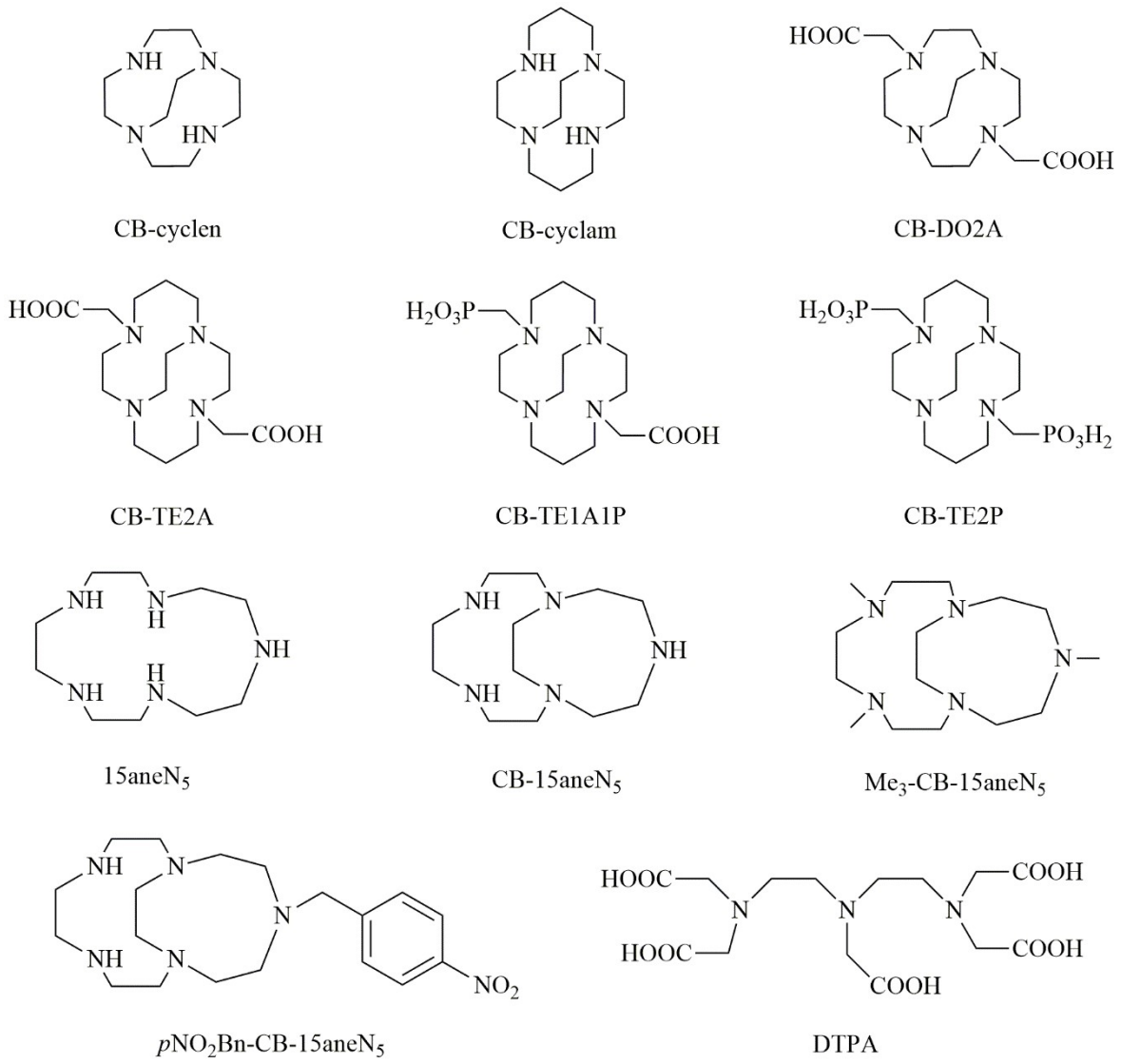

Scheme S1. Structures of the ligands mentioned in the paper.

Table S1. The inertness of some Cu(II) complexes formed with highly rigid azamacrocycles.

Complexes	Half-life ($t_{1/2}$)
[Cu(CB-DO2A)]	< 3 min (at 90 °C)[a]
[Cu(CB-TE2A)]	154 h (at 90 °C)[b]
$[Cu(CBTE1A1P)]^{-}$	6.8 h (at 90 °C)[b]
$[Cu(CB\text{-}TE2P)]^{2-}$	3.8 h (at 90 °C)[b]
$[Cu(15aneN_5)]^{2+}$	< 2 min (at 50 °C)[c]
$[Cu(Me_3\text{-}CB\text{-}15aneN_5)]^{2+}$	5.3 d (at 50 °C)[c]
$[Cu(CB\text{-}15aneN_5)]^{2+}$	8 min (at 50 °C)
$[Cu(p NO_2Bn\text{-}CB\text{-}15aneN_5)]^{2+}$	2.3 h (at 50 °C)

a) Ref.[1], b) Ref.[2], c) Ref.[3]

Synthesis of the ligands

General procedures

Commercial reagents/solvents purchased from Sigma-Aldrich (St. Louis, MO, USA), Merck KGaA (Darmstadt, Germany) and Tokyo Chemical Industry (Tokyo, Japan) were used without further purification. The microwave activation was accomplished by a CEM Microwave Synthesis System (Discover-S #908860) including an Explorer 48 #909480 autosampler. The synthetic reactions were followed by using a Waters Alliance 2690 HPLC unit equipped with Waters 996 PDA detector, and a Phenomenex C18(2) 150*4.6 mm 3 micron column. The preparative HPLC separations were carried out with a YL9100 HPLC system (Korea) equipped YL9101S degasser, YL9110S pump, YL9120S UV/VIS detector, Phenomenex Luna Prep C18(2) 100A 250x21.20 mm 10 micron 00G-4324-P0 column and Sigma-Aldrich CHROMASOLV® Plus solvents. The NMR measurements were carried out with *Bruker* DRX *360 MHz and Bruker Avance I 400 MHz* spectrometers using deuterated solvents. Mass spectra were recorded on a maXis II UHR ESI-QTOF MS Bruker instrument in the Laboratory of Instrumental Analysis, Department of Inorganic and Analytical Chemistry of the University of Debrecen. The purity of the product was >99.8% determined by reverse-phase HPLC with UV−Vis detection at 220 and 260 nm.

Table S2. Applied gradient flow of analytical HPLC (Column: Luna C18(2) 150 mm×4.6 mm, 100 Å, 3 μm).

	A solvent (MeCN)	***B solvent*** (5 mM TFA solution)
0.0 min	20 %	80 %
15.0 min	90 %	10 %
16.0 min	20 %	80 %

3,6-Di(tosyl)-3,6-diazaoctane-1,8-di(toluene-4-sulfonate) (2):

Solid NaOH (6.75 g, 0.169 mol, 5.0 eq.) was dissolved in 100 ml distilled water in a beaker. The N,N'-bis(2-hydroxyethyl)ethylenediamine (***1***, 5.00 g, 33.8 mmol, 1.0 eq.) was added dropwise to the basic solution which was stirred. Para-toluenesulfonyl chloride (32.1 g, 0.169 mol, 5.0 eq.) was diluted in 150 mL diethyl-ether and it was added dropwise to the aqueous solution. After the addition the reaction was stirred strongly so the ether could vaporize freely from the reaction mixture. After one hour, white precipitate appeared. The mixture was cooled to near 5 °C overnight and the excess water was decantated from above the precipitate. The solid was suspended with 50 mL fresh distilled water. This mixture was stirred over 2 hours, after then it was filtrated. The white solid was washed subsequently with cold water and cold diethyl-ether and dried under vacuum. The product was a white powder (23.5 g, 91 % yield). ^{1}H-NMR (400 MHz, $CDCl_3$): δ (ppm) 7.76 (4H, d, *J*=8.4 Hz, aromatics), 7.71 (4H, d, *J*=8.4 Hz, aromatics), 7.33 (8H, d, *J*=8.4 Hz, aromatics), 4.13 (4H, t, *J*=5.3 Hz, -CH_2-), 3.35 (4H, t, *J*=5.3 Hz, -CH_2-), 3.29 (4H, s, -CH_2-), 2.43 (12H, s, -CH_3); ^{13}C-NMR (100 MHz, $CDCl_3$): δ (ppm) 145.3, 144.1, 135.1, 132.5 (4x2C, *Cq*-aromatics), 130.1, 128.1, 127.5 (2x4C + 1x8C, aromatics), 69.1, 50.0, 49.6 (3x2C, -*C*H_2-), 21.7 (4x1C, -*C*H_3); ESI-MS (m/z, positive mode): $[M+Na]^+_{calc.}$: 787.1458, $[M+Na]^+_{found}$: 787.1463.

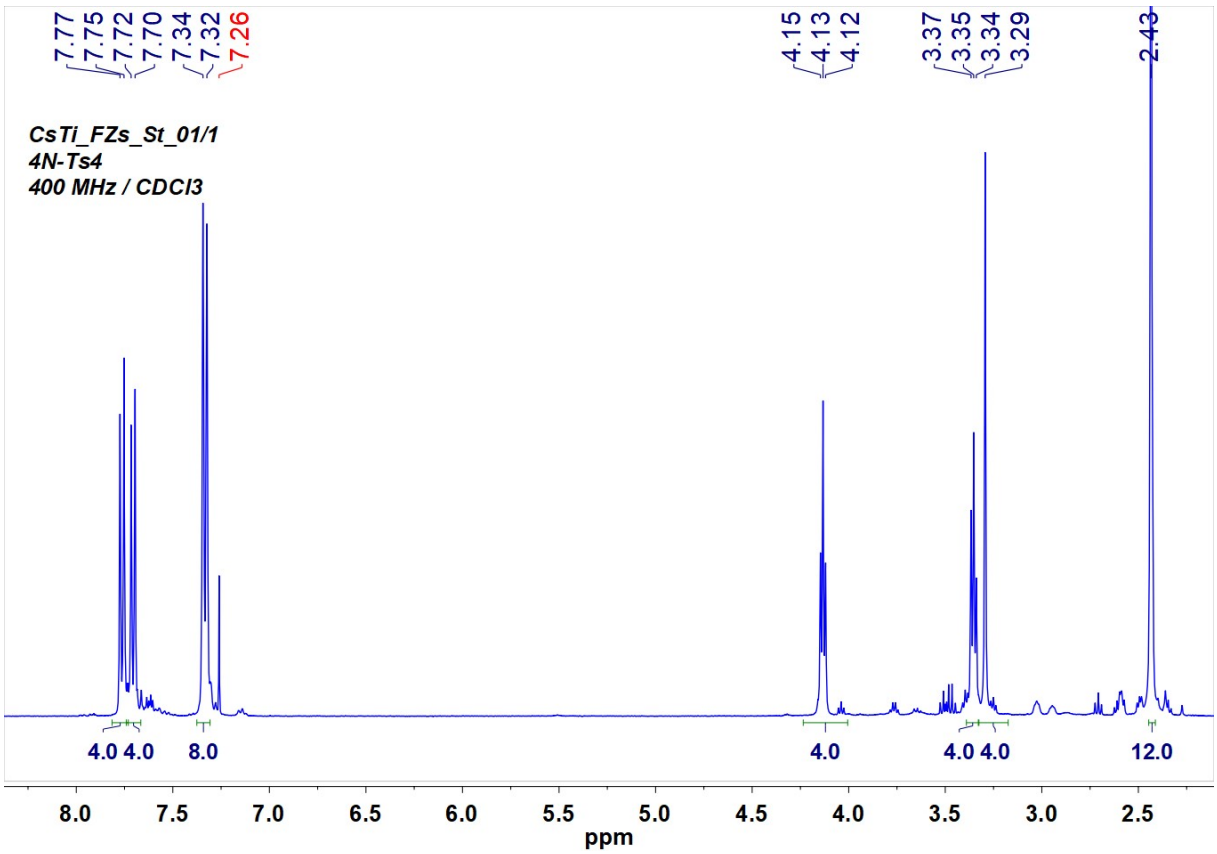

Figure S1. [1]H-NMR spectrum of 3,6-di(tosyl)-3,6-diazaoctane-1,8-di(toluene-4-sulfonate) (2) (Reference: $CDCl_3$).

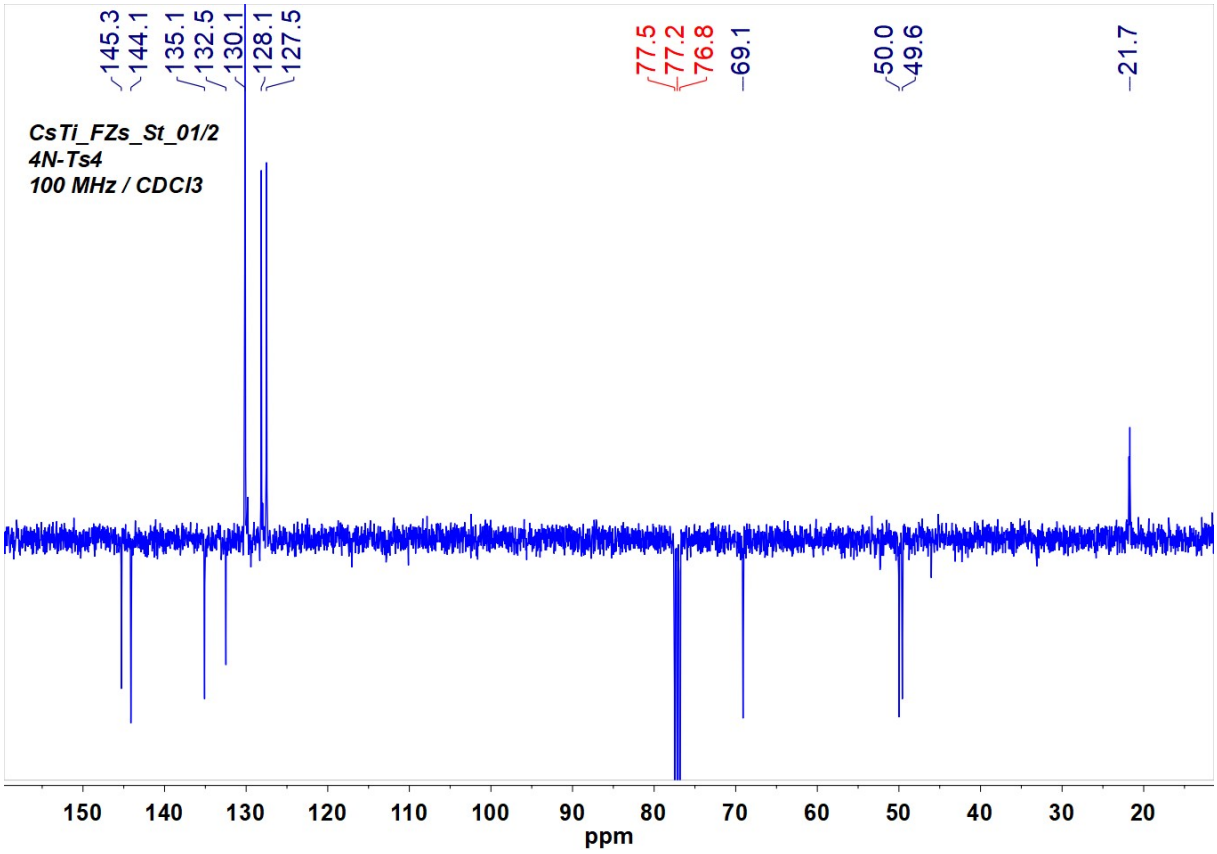

Figure S2. [13]C-NMR spectrum of 3,6-di(tosyl)-3,6-diazaoctane-1,8-di(toluene-4-sulfonate) (2) (Reference: $CDCl_3$).

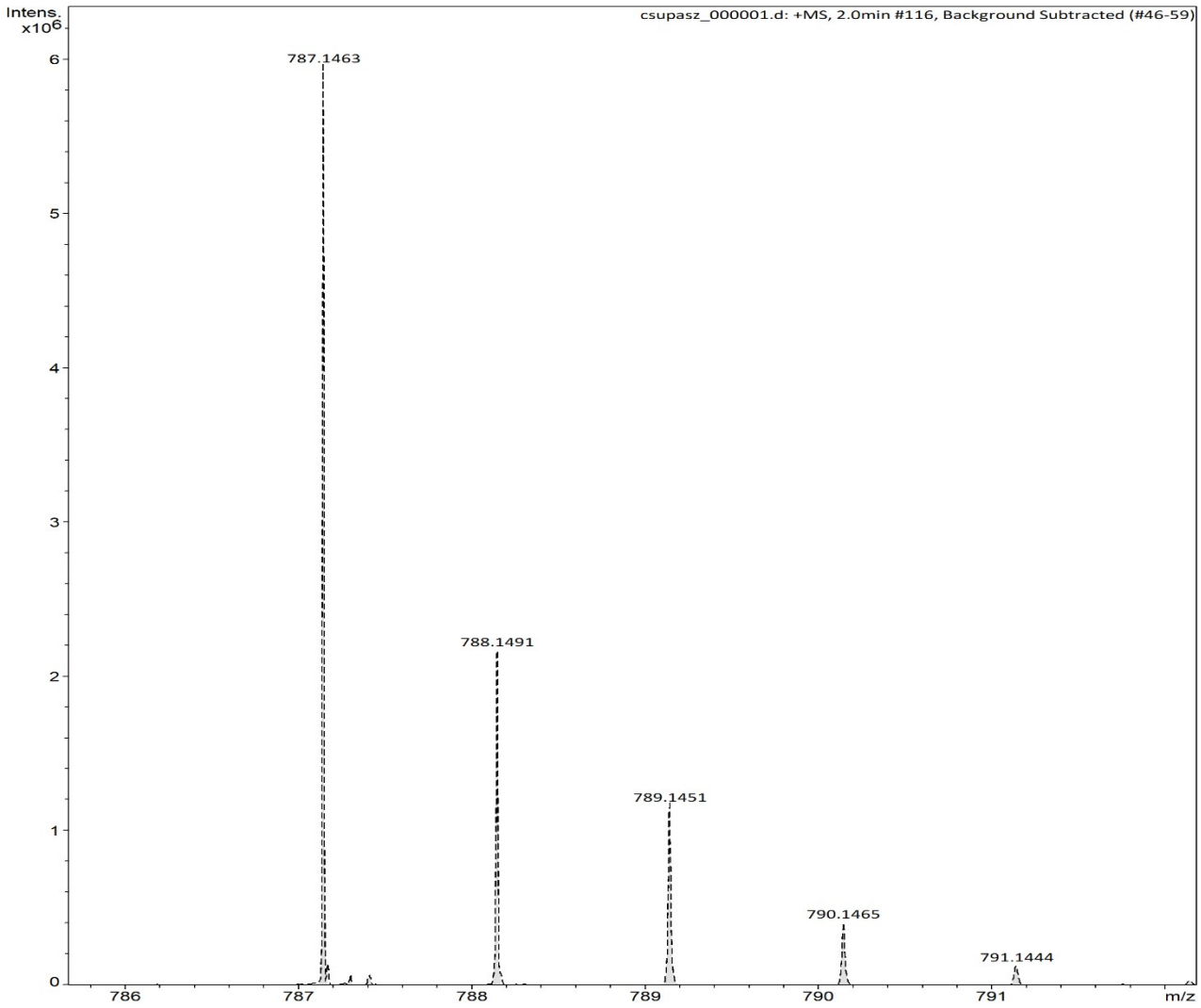

Figure S3. MS spectrum of 3,6-di(tosyl)-3,6-diazaoctane-1,8-di(toluene-4-sulfonate) (2).

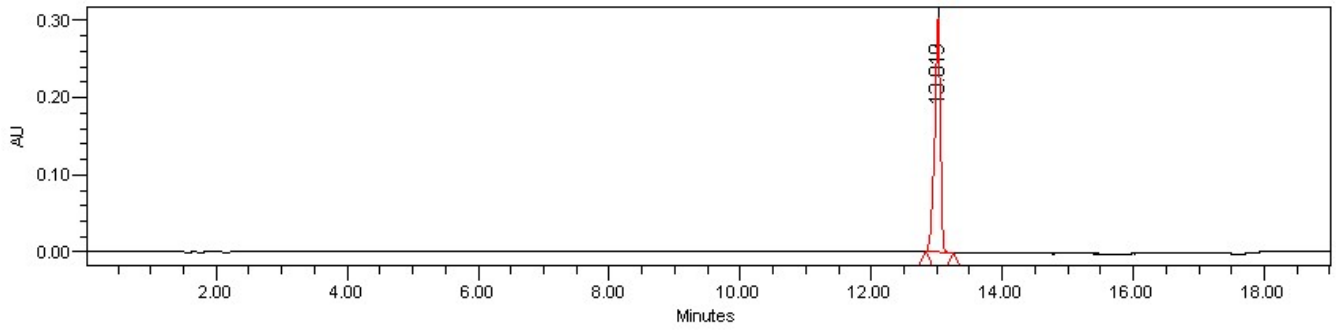

Figure S4. Analytical HPLC chromatogram of 3,6-di(tosyl)-3,6-diazaoctane-1,8-di(toluene-4-sulfonate) (2) (t_R=13.01 min).

***4,7-Di(tosyl)-1,4,7,10,13-pentaazabicyclo[8.5.2]heptadecane (4)*:**

1,4,7-triazacyclononane (***3***, 0.20 g, 1.55 mmol, 1.0 eq.) was measured into a two-necked flask and dissolved in 20 mL dry acetonitrile. K_2CO_3 (427 mg, 3.10 mmol, 2.0 eq.) was suspended in the solution. The flask was connected to a condenser and the mixture was heated to 60 °C. The protected diamine (***2***, 1.18 g, 1.55 mmol, 1.0 eq.) was measured into a dropping funnel in 60 mL dry acetonitrile. This mixture was added dropwise slowly to the hot reaction mixture which was stirred for 1 day. (The reaction was followed by analytical HPLC method). After completion of the reaction the hot mixture was filtered through a G3 glass filter and the solvent from the filtrate was removed under reduced pressure. The product was recrystallized

from 5 mL acetonitrile as colorless powder by keeping the solution in a fridge for 1 day. (545 mg, 64 % yield). ^{1}H-NMR (400 MHz, $CDCl_3$): δ (ppm) 7.70 (4H, d, *J*=8.4 Hz, aromatics), 7.33 (4H, d, *J*=8.4 Hz, aromatics), 4.15, 3.29, 3.18, 3.07 (4x2H, dd, -C*H*$_2$-), 2.88 (2H, dd, -C*H*$_2$-), 2.72 (2H, dd, -C*H*$_2$-), 2.64 (4H, m, -C*H*$_2$-), 2.54 (4H, dt, -C*H*$_2$-), 2.46-2.41 (8H, m, -C*H*$_2$- + -C*H*$_3$), 2.30 (2H, dd, -C*H*$_2$-); ^{13}C-NMR (100 MHz, $CDCl_3$): δ (ppm) 143.6, 135.6 (2x2C, *Cq*-aromatics), 129.9, 127.5 (2x4C, aromatics), 59.9, 52.1, 51.8, 49.6, 48.4, 45.4 (6x2C, -*C*H$_2$-), 21.7 (2x1C, -CH$_3$); ESI-MS (m/z, positive mode): $[M+H]^+_{calc.}$: 550.2516, $[M+H]^+_{found}$: 550.2516.

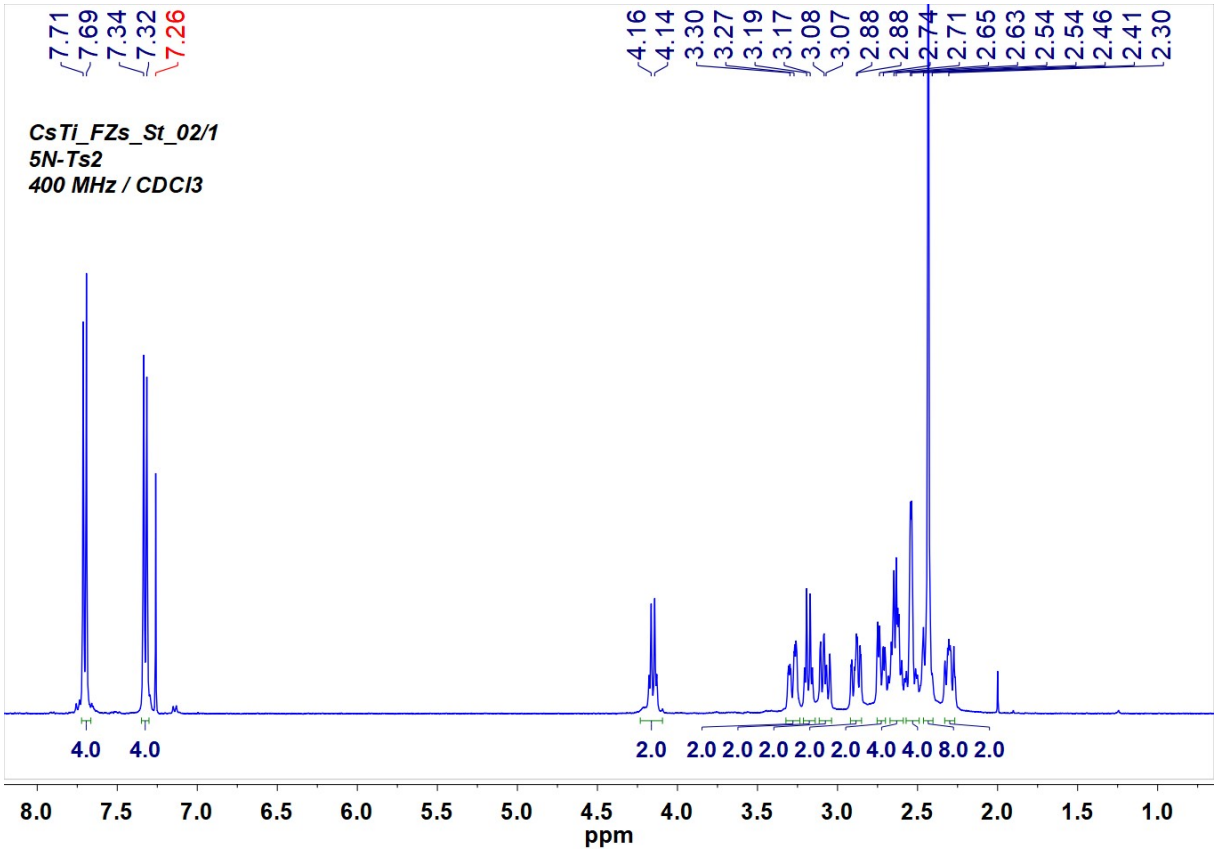

Figure S5. ^{1}H-NMR spectrum of 4,7-di(tosyl)-1,4,7,10,13-pentaazabicyclo[8.5.2]heptadecane (4) (Reference: $CDCl_3$).

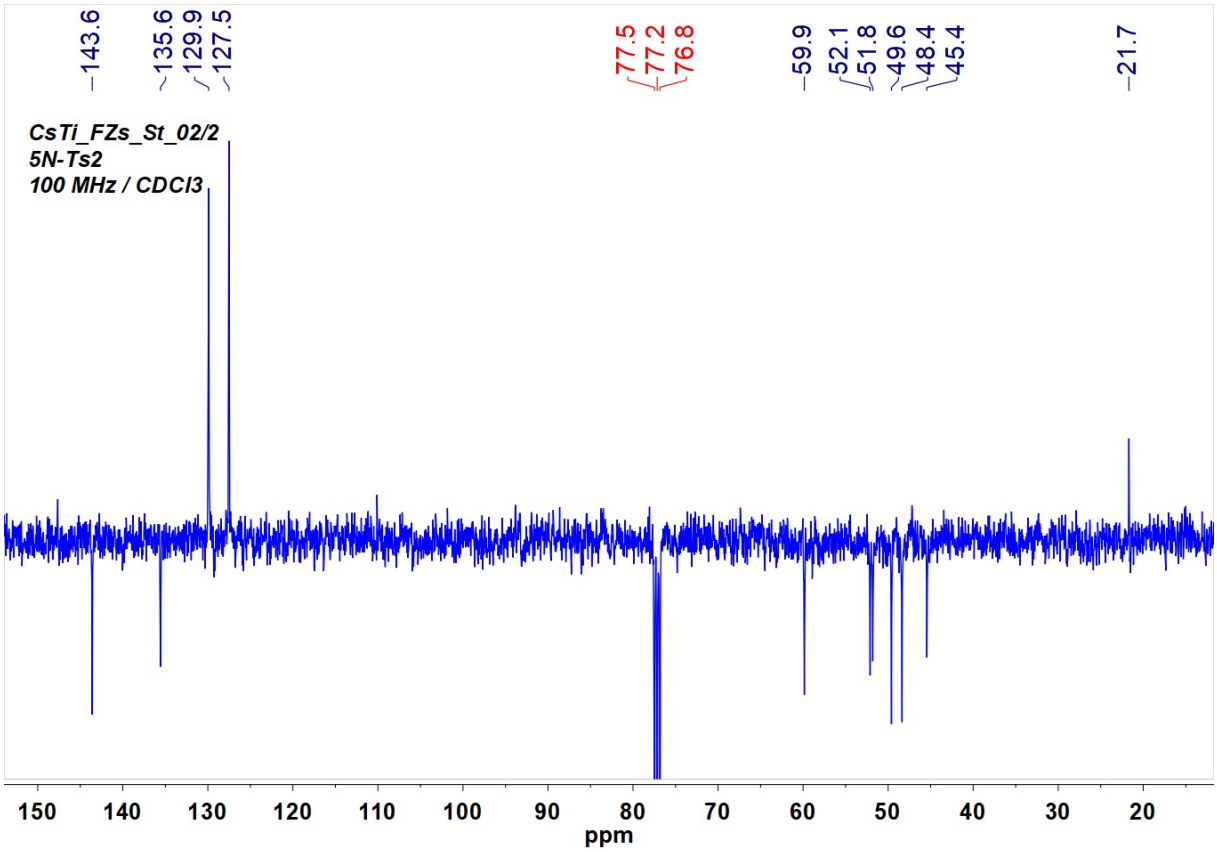

Figure S6. ^{13}C-NMR spectrum of 4,7-di(tosyl)-1,4,7,10,13-pentaazabicyclo[8.5.2]heptadecane (4) (Reference: $CDCl_3$).

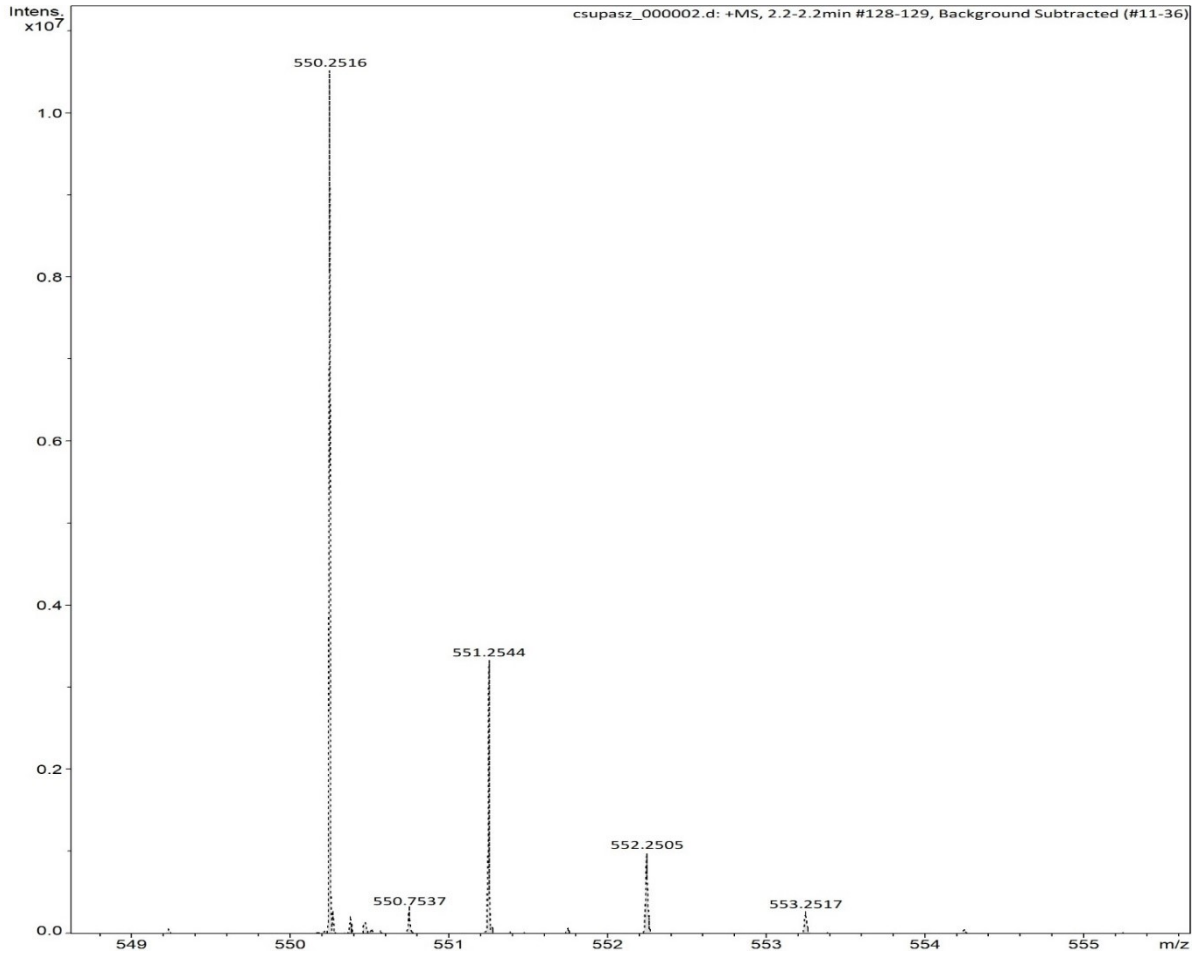

Figure S7. MS spectrum of 4,7-di(tosyl)-1,4,7,10,13-pentaazabicyclo[8.5.2]heptadecane (4).

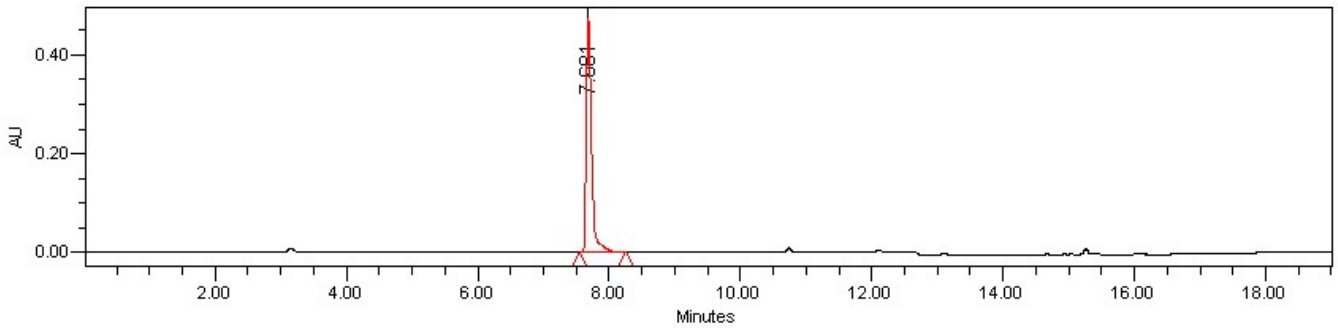

Figure S8. Analytical HPLC chromatogram of 4,7-di(tosyl)-1,4,7,10,13-pentaazabicyclo[8.5.2]heptadecane (4) (t_R=7.68 min).

1,4,7,10,13-Pentaazabicyclo[8.5.2]heptadecane (5):

1,4,7-Di(tosyl)-1,4,7,10,13-pentaazabicyclo[8.5.2]heptadecane (***4***, 500 mg, 0.910 mmol, 1.0 eq.) was dissolved in 4.00 mL concentrated sulfuric acid. The reaction was performed in microwave reactor (120 °C, 20 W, 60 min.). Subsequently, the mixture was cooled to near 0 °C. The cold mixture was poured into 100 ml cold diethyl-ether and a white precipitate appeared. The acidic ether was decanted from above the solid. The product was dissolved in 5 mL distilled water and the pH of the solution was adjusted to 7.0. The compound was purified by preparative HPLC method. The product was colorless oil (123 mg, 56 % yield). ^{1}H-NMR (360 MHz, D_2O): δ (ppm) 3.24-3.16 (4H, m, -C*H*$_2$-), 3.14-2.98 (8H, m, -C*H*$_2$-), 2.96-2.88 (8H, m, -C*H*$_2$-), 2.86-2.76 (4H, m, -C*H*$_2$-); ^{13}C-NMR (90 MHz, CD_3OD): δ (ppm) 54.2, 50.3, 50.0, 44.5, 44.4, 43.6 (6x2C, -*C*H$_2$); ESI-MS (m/z, positive mode): $[M+H]^+_{calc.}$: 242.2339, $[M+H]^+_{found}$: 242.2339.

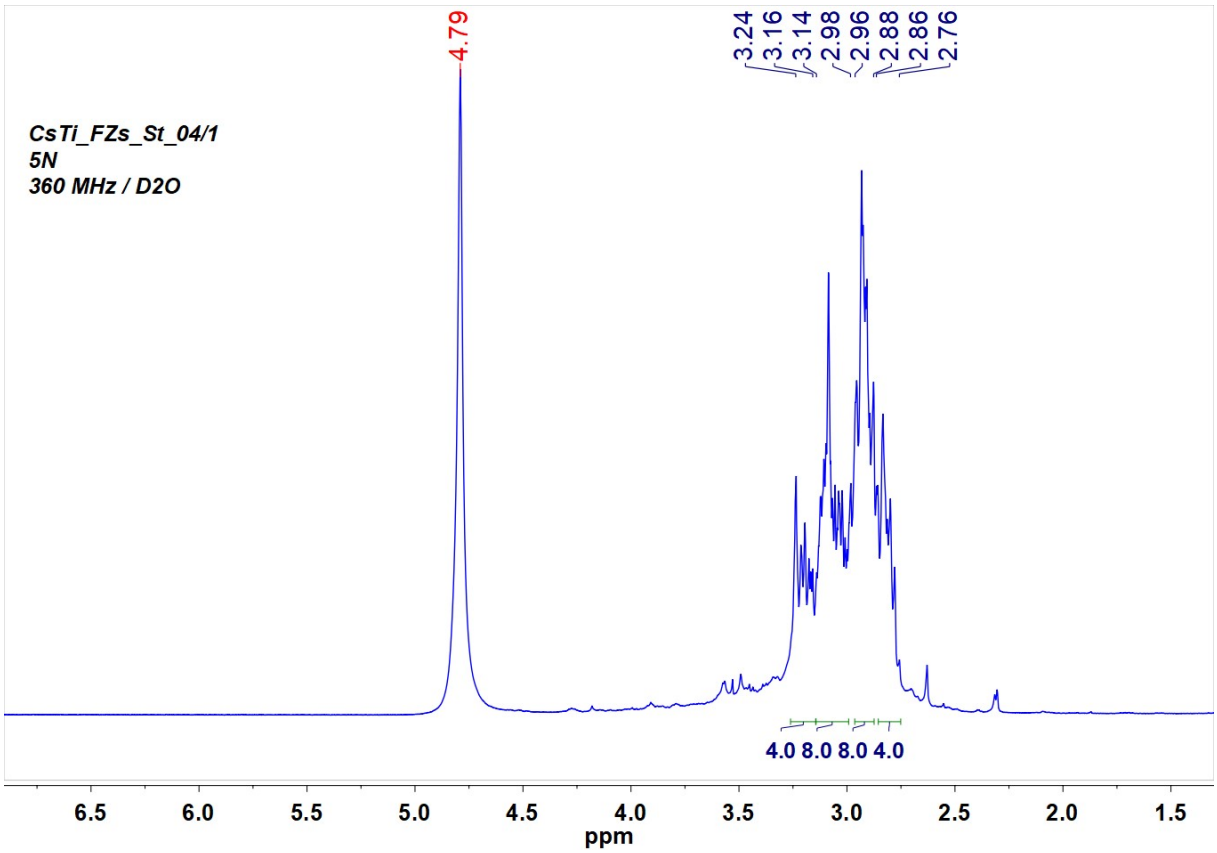

Figure S9. ^{1}H-NMR spectrum of 1,4,7,10,13-pentaazabicyclo[8.5.2]heptadecane (5) (Reference: D_2O).

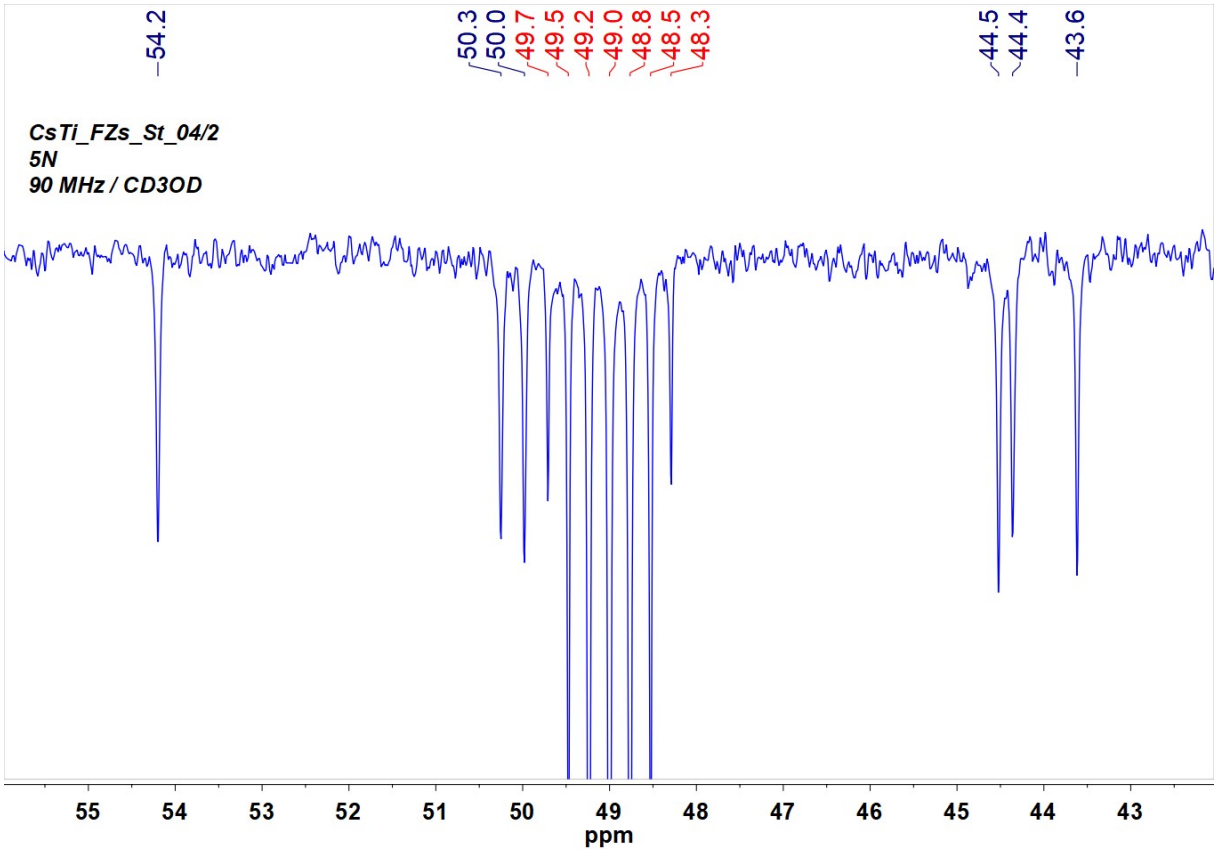

Figure S10. ^{13}C-NMR spectrum of 1,4,7,10,13-pentaazabicyclo[8.5.2]heptadecane (5) (Reference: CD_3OD).

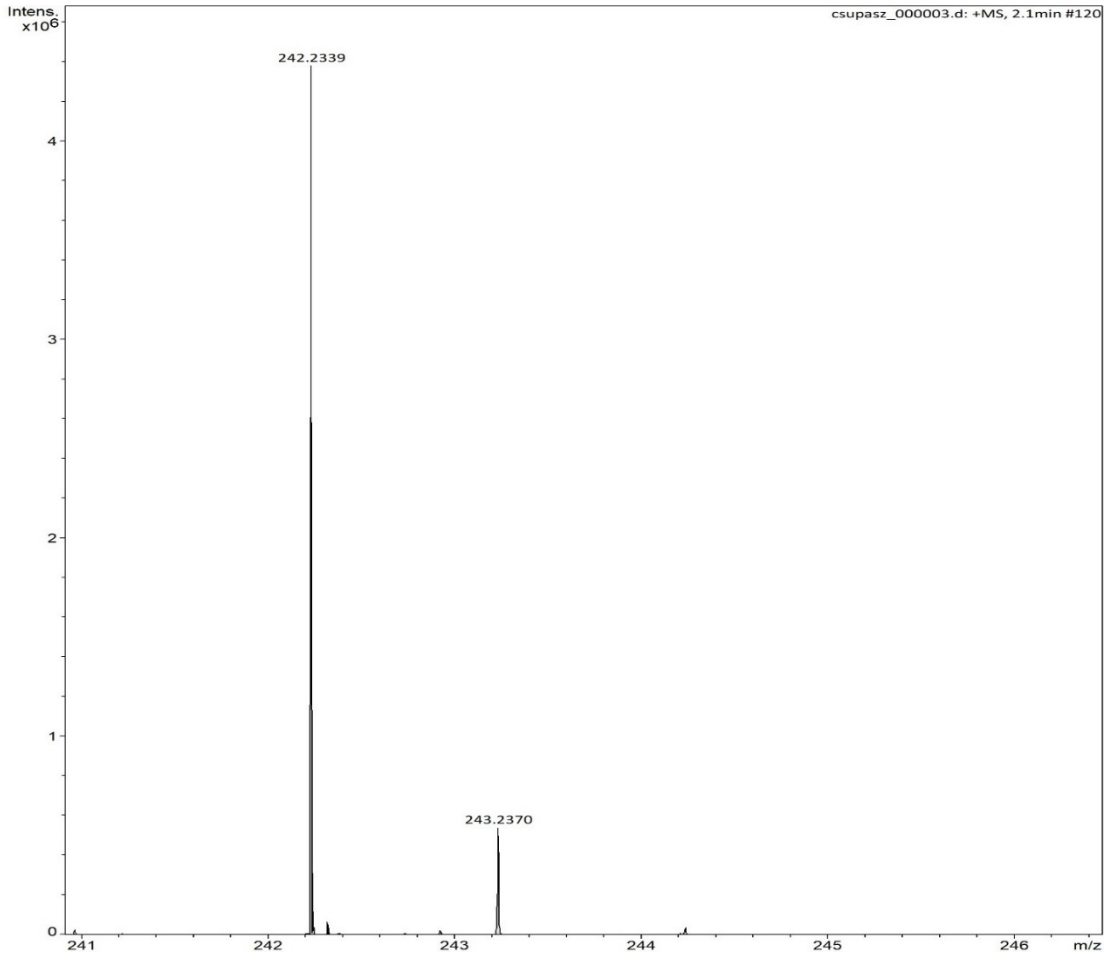

Figure S11. MS spectrum of 1,4,7,10,13-pentaazabicyclo[8.5.2]heptadecane (5).

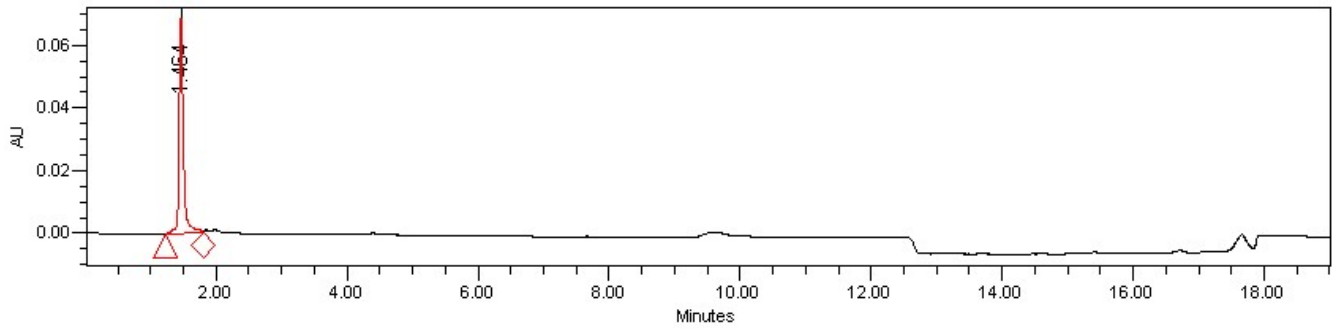

Figure S12. Analytical HPLC chromatogram of 1,4,7,10,13-pentaazabicyclo[8.5.2]heptadecane (5) (t_R=1.46 min).

13-(4-Nitrobenzyl)-4,7-ditosyl-1,4,7,10,13-pentaazabicyclo[8.5.2]heptadecane (7):

4,7-Di(tosyl)-1,4,7,10,13-pentaazabicyclo[8.5.2]heptadecane (***4***, 350 mg, 0.637 mmol, 1.0 eq.) and K_2CO_3 (132 mg, 0.955 mmol, 1.5 eq.) were added to a two-neck flask and the mixture was suspended in 60 ml dry acetonitrile. The reaction was stirred at reflux temperature under argon atmosphere. 4-nitrobenzyl bromoacetate (***6***, 151 mg, 0.70 mmol, 1.1 eq.) was dissolved in 60 ml dry acetonitrile and this solution was added dropwise to the heated reaction mixture. The reaction was monitored by analytical HPLC method and the precipitate was filtered off after completion. The solvent from the filtrate was removed under reduced pressure and the residue was used directly for the next reaction without any further purification. The product was a slightly orange oil (420 mg, 96 % yield). ^{1}H-NMR (360 MHz, $CDCl_3$): δ (ppm) 8.16 (2H, d, *J*=8.4 Hz, aromatics), 7.65 (4H, d, *J*=8.4 Hz, aromatics), 7.56 (4H, d, *J*=8.4 Hz, aromatics), 7.40 (2H, d, *J*=8.4 Hz, aromatics), 4.11 (2H, s, -CH_2-), 3.53 (4H, m, -CH_2-), 3.38-3.34 (8H, m, -CH_2-), 3.24 (4H, m, -CH_2-), 3.05 (4H, m, -CH_2-), 2.87 (2H, d, -CH_2-), 2.47-2.44 (8H, m, -CH_2- + -CH_3); ^{13}C-NMR (90 MHz, $CDCl_3$): δ (ppm) 147.8, 145.4, 144.4, 131.4 (2x1C + 2x2C, *Cq*-aromatics), 130.8, 130.4, 128.4, 123.9 (2x2C + 2x4C, aromatics), 58.9, 56.1, 53.2, 51.1, 50.6, 49.2, 48.7 (1x1C + 6x2C, -CH_2-), 21.8 (2x1C, -CH_3); ESI-MS (m/z, positive mode): $[M+H]^+_{calc.}$: 685.2837, $[M+H]^+_{found}$: 685.2836.

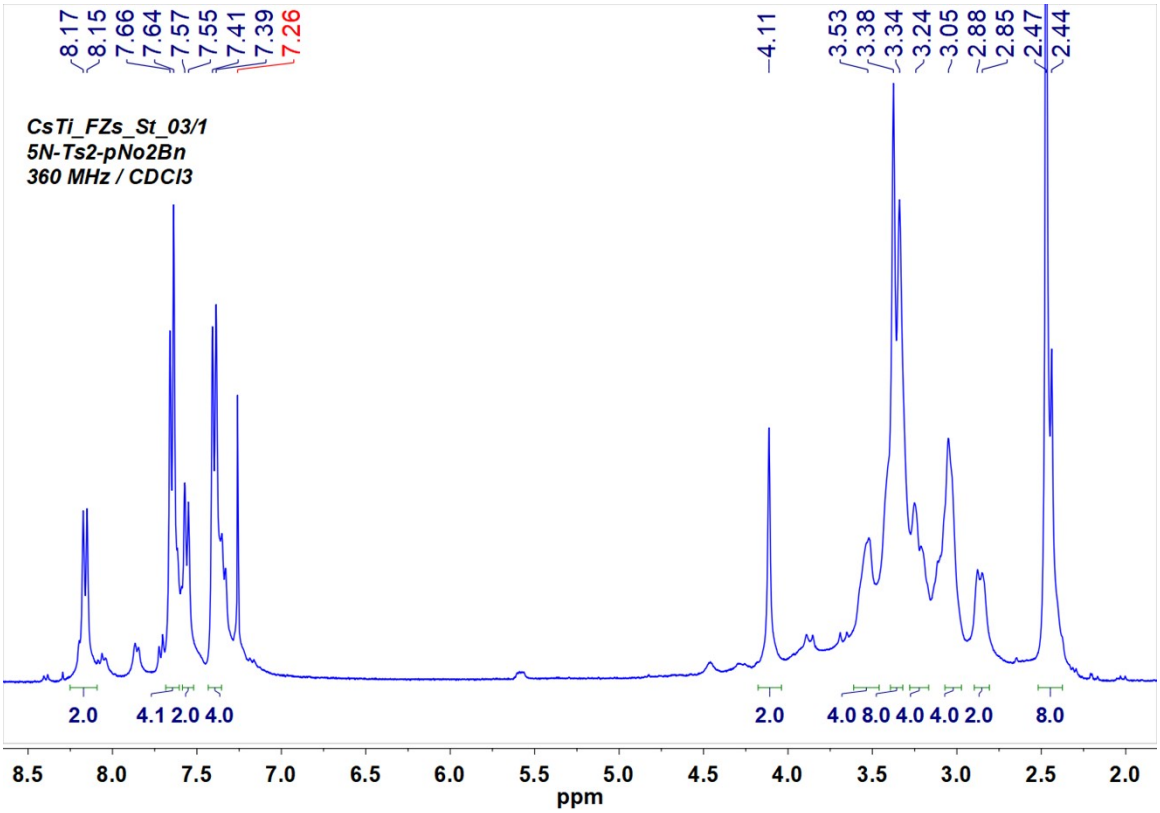

Figure S13. ^{1}H-NMR spectrum of 13-(4-nitrobenzyl)-4,7-ditosyl-1,4,7,10,13-pentaazabicyclo[8.5.2]heptadecane (7) (Reference: $CDCl_3$).

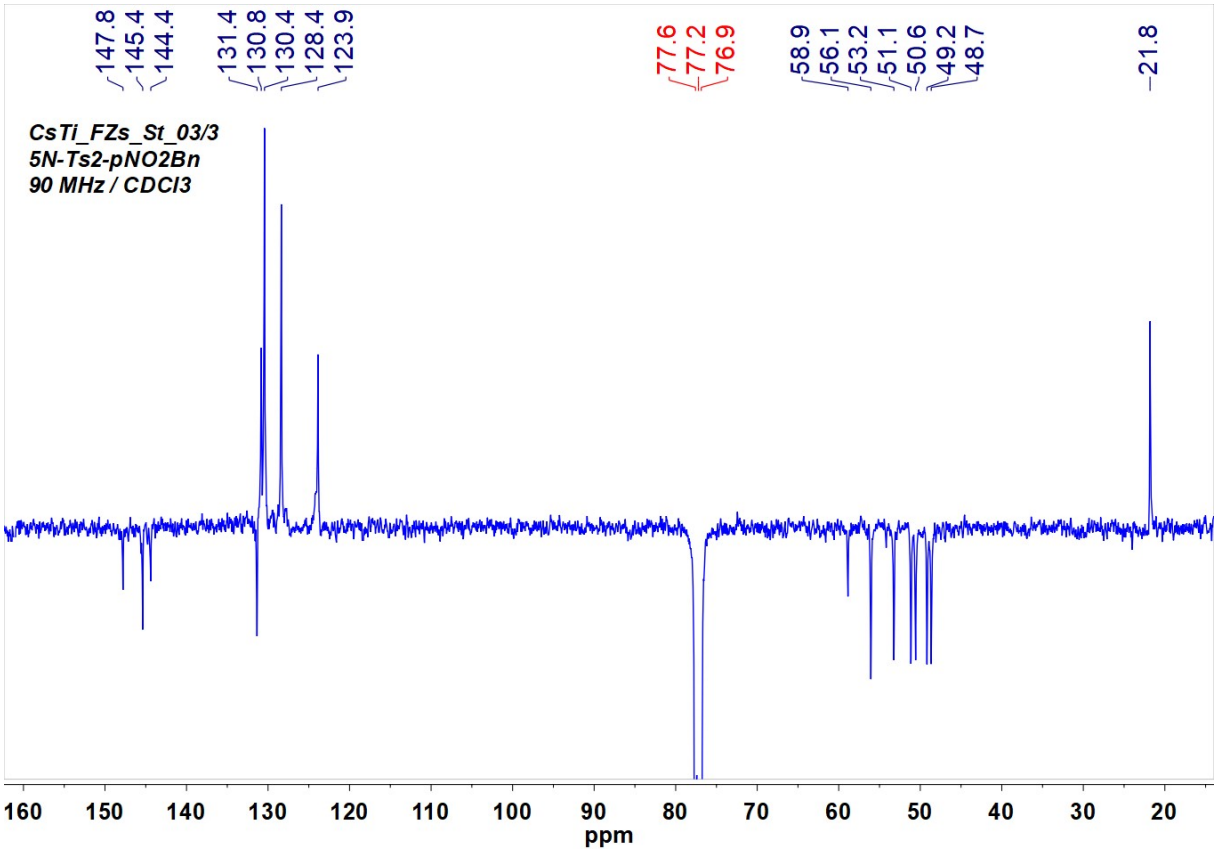

Figure S14. ^{13}C-NMR spectrum of 13-(4-nitrobenzyl)-4,7-ditosyl-1,4,7,10,13-pentaazabicyclo[8.5.2]heptadecane (7) (Reference: $CDCl_3$).

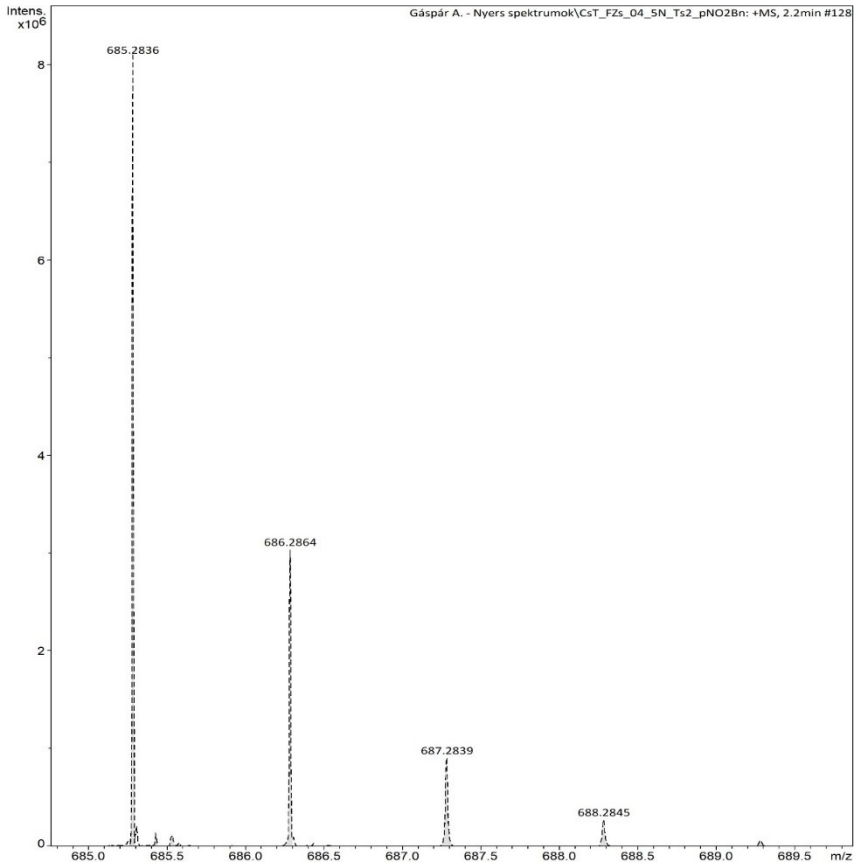

Figure S15. MS spectrum of 13-(4-nitrobenzyl)-4,7-ditosyl-1,4,7,10,13-pentaazabicyclo[8.5.2]heptadecane (7).

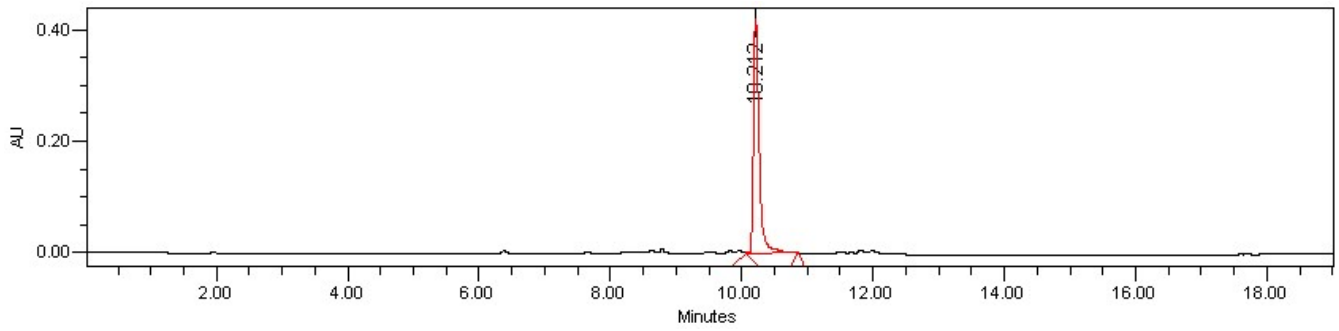

Figure S16. Analytical HPLC chromatogram of 13-(4-nitrobenzyl)-4,7-ditosyl-1,4,7,10,13-pentaazabicyclo[8.5.2]heptadecane (7) (t_R=10.21 min).

13-(4-Nitrobenzyl)-1,4,7,10,13-Pentaazabicyclo[8.5.2]heptadecane (8):

13-(4-Nitrobenzyl)-4,7-ditosyl-1,4,7,10,13-pentaazabicyclo[8.5.2]heptadecane (*7*, 650 mg, 0.950 mmol, 1.0 eq.) was dissolved in 2.00 mL concentrated sulfuric acid. The reaction was performed in microwave reactor (120 °C, 20 W, 90 min.), and then was cooled to near 0 °C. After pouring the cold mixture into 100 ml cold diethyl-ether, a brown precipitate appeared. The acidic ether was decanted from above the solid and which was dissolved in 5 mL distilled water. The pH of this solution was adjusted to near 7.0 and the compound was purified by preparative HPLC method. The product was an orange oil. (232 mg, 65 % yield) ^{1}H-NMR (400 MHz, CD_3CN): δ (ppm) 8.22 (2H, d, *J*=8.4 Hz, aromatics), 7.58 (2H, d, *J*=8.4 Hz, aromatics), 4.03 (2H, s, -C*H*$_2$-), 3.25 (4H, dd, -C*H*$_2$-), 3.16-3.04 (8H, m, -C*H*$_2$-), 2.99-2.83 (10H, m, -C*H*$_2$-) 2.68 (2H, m, -C*H*$_2$-); ^{13}C-NMR (90 MHz, D_2O): δ (ppm) 147.4, 140.3 (2x1C, *Cq*-aromatics), 131.2, 123.7 (2x2C, aromatics), 58.3, 52.8, 50.2, 48.2, 47.2, 42.8, 41.7 (1x1C + 6x2C, -*C*H$_2$-); ESI-MS (m/z, positive mode): $[M+H]^+_{calc.}$: 377.2660, $[M+H]^+_{found}$: 377.2660.

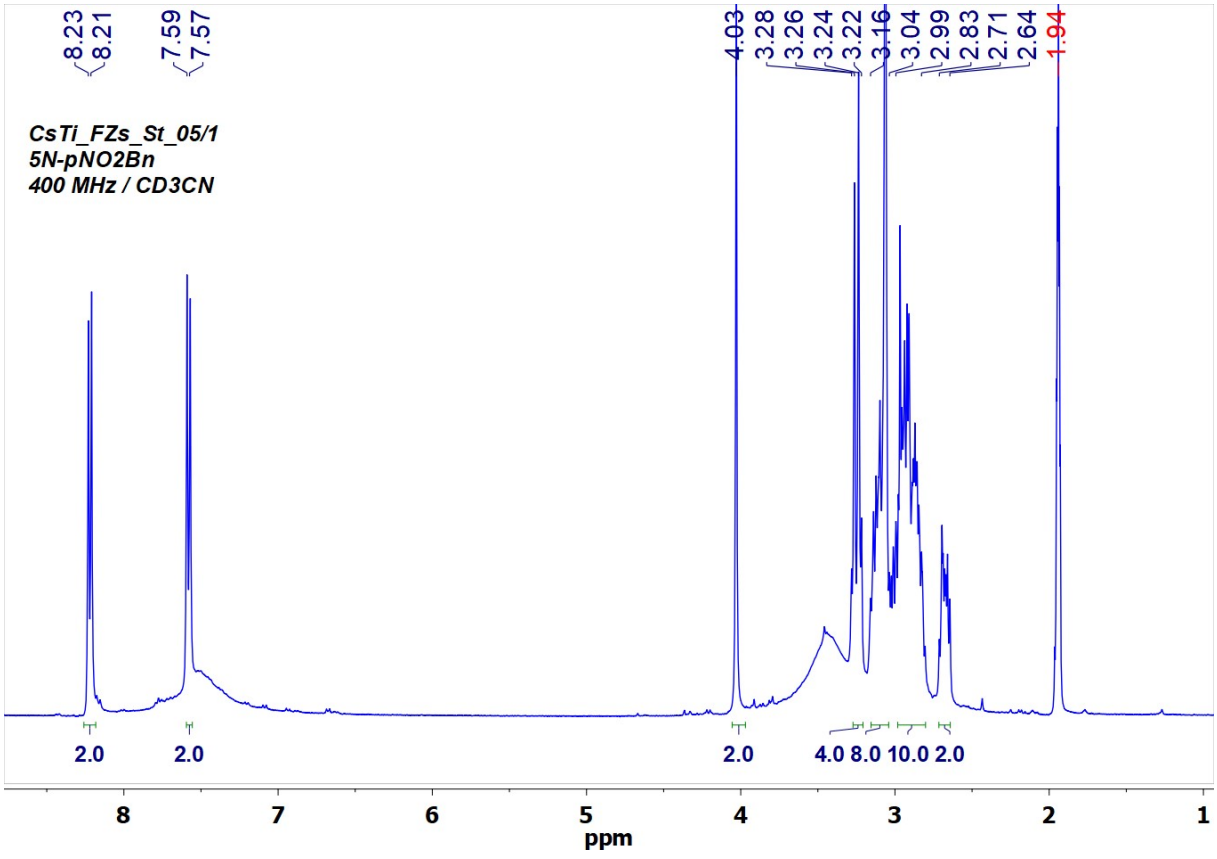

Figure S17. ^{1}H-NMR spectrum of 13-(4-nitrobenzyl)-1,4,7,10,13-pentaazabicyclo[8.5.2]heptadecane (8) (Reference: CD_3CN).

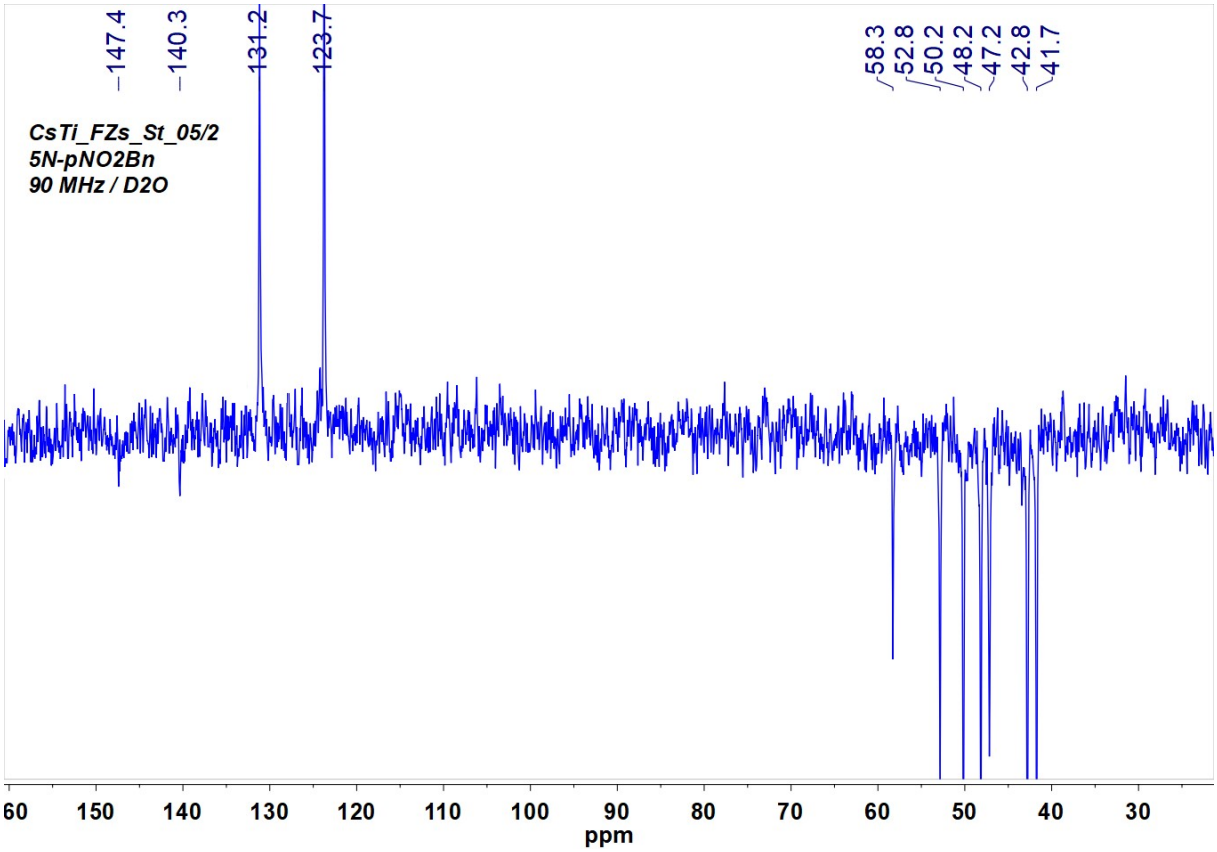

Figure S18. ^{13}C-NMR spectrum of 13-(4-nitrobenzyl)-1,4,7,10,13-pentaazabicyclo[8.5.2]heptadecane (8) (Reference: TMS).

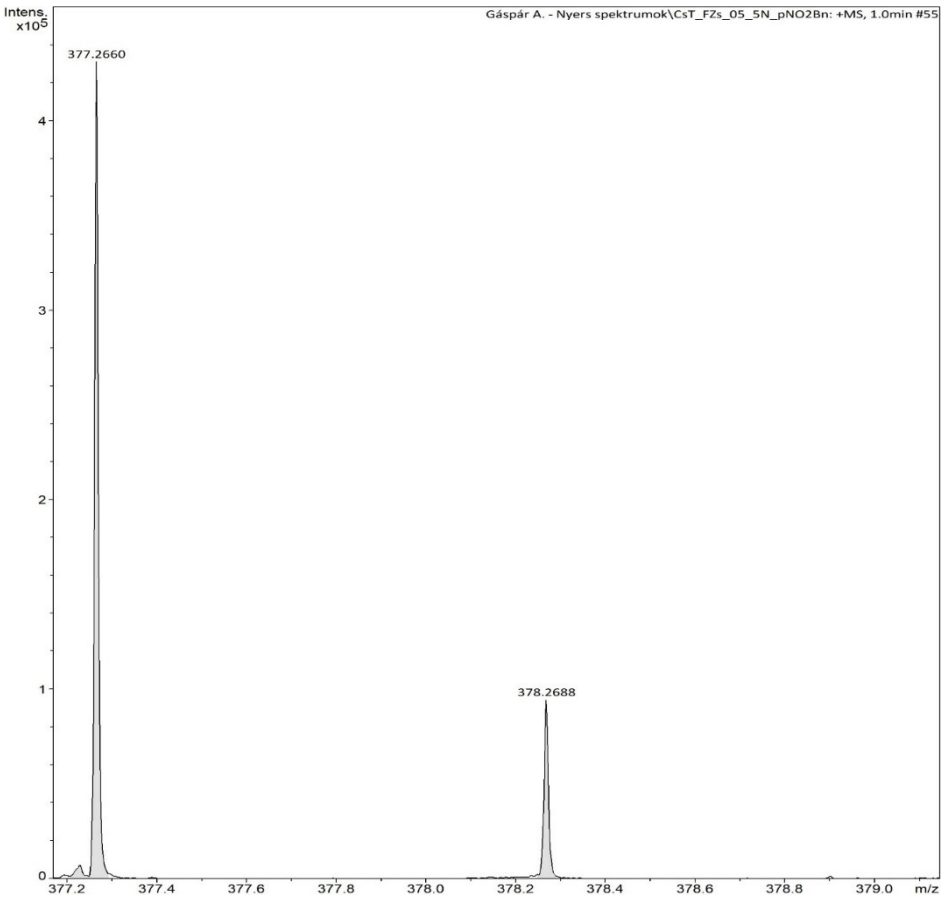

Figure S19. MS spectrum of 13-(4-nitrobenzyl)-1,4,7,10,13-pentaazabicyclo[8.5.2]heptadecane (8).

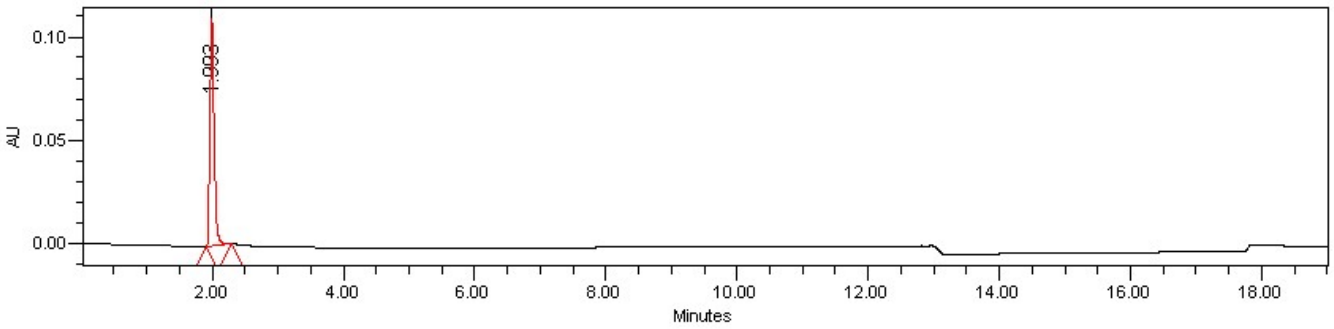

Figure S20. Analytical HPLC chromatogram of 13-(4-nitrobenzyl)-1,4,7,10,13-pentaazabicyclo[8.5.2]heptadecane (8) (t_R=1.90 min).

Equilibrium studies

The highest analytical grade chemicals were used for the experiments. Complexometric titrations were carried out with standardized Na_2H_2EDTA solution in the presence of murexid indicator to determine the concentration of the $CuCl_2$ stock solution in the presence of murexid.

pH-potentiometric studies

A *Methrohm 888 Titrando* titration workstation equipped with a *Metrohm-6.0233.100* combined electrode was applied to perform the pH-potentiometric titrations. The electrode was calibrated with two point calibration method using KH-phthalate (pH=4.005) and borax (pH=9.177) as standards. The titrated samples (6.0 mL) were kept under inert (N_2) atmosphere. The solutions were stirred and thermostated (25 °C) during the titration. The ionic strength was set to 1.0 M (NaCl). The solutions containing the ligand in 2.00 mM concentration were titrated with standardized 0.2 M NaOH solution. The protonation constants were estimated by evaluating 180-300 volume of the titrating solution – pH data pairs in the pH range of 1.7-12.0.

The protonation constants of the ligands (Equation S1) as well as the stability constant of the $[Cu(CB\text{-}15aneN_5)]^{2+}$ complex (Equation S2) are defined as follows:

$$K_i^H = \frac{[H_iL]}{[H_{i-1}L][H^+]} \qquad i=1\text{-}3 \tag{S1}$$

$$K_{ML} = \frac{[ML]}{[M][L]} \tag{S2}$$

The pH read-out was converted into $[H^+]$ from using the method of *Irving et al*. by titrating 0.01 M HCl solution (1.0 M NaCl) with 0.2 M NaOH solution.[4] The value of K_w (ionic product of water) was calculated from the same titration (pK_w=13.81). The PSEQUAD program was used to evaluate the equilibrium constants.[5]

Spectrophotometry

Due to the high thermodynamic stability of $[Cu(CB\text{-}15aneN_5)]^{2+}$ the complex formation is complete under acidic conditions, pH < 2.0. For this reason, 8 batch samples ($c_{lig}=c_{Cu(II)}$=0.200 mM, I=1.0 M (NaCl+HCl), 25 °C) were prepared in the acidic concentration range, from 0.1 to 1.0 M . The ionic strength in the samples was set to 1.0 M by NaCl ($[H^+]+[Na^+]$=1 M). The samples were set aside for two months to attain the equilibrium at 25 °C and the absorption spectra were recorded in the range of 200-350 nm using quarts cuvettes (1.000 cm optical path length) via Cary 100 BIO UV-Vis spectrophotometer. The absorbance recorded at 280, 285, 290, 295 and 300 nm were used in the fitting procedure.

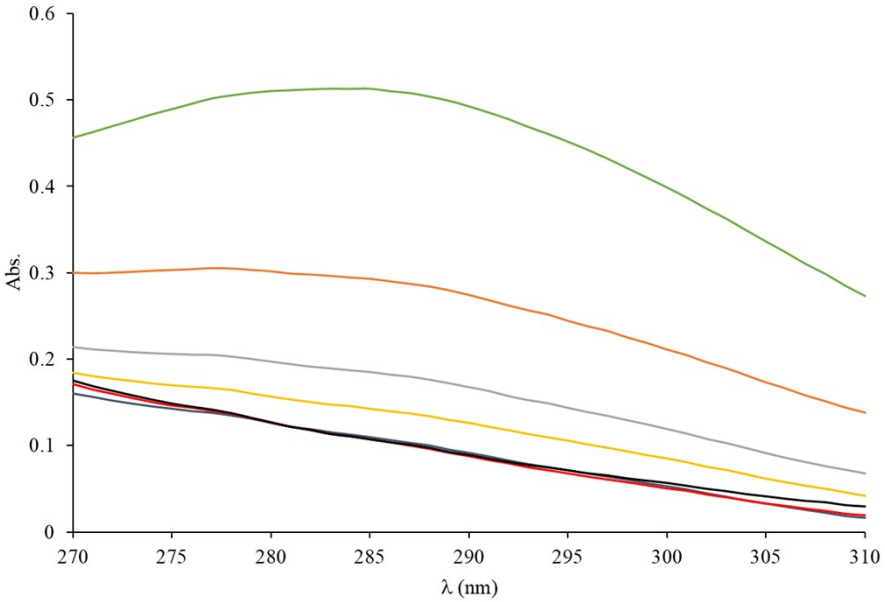

Figure S21. Absorption spectra as a function of acid concentration recorded in the Cu(II)– CB-15aneN$_5$ system. $c_{Cu(II)}$= $c_{CB\text{-}15aneN5}$= 0.2 mM, c_{Cl^-}= 1 M, [H^+] = 1.041, 0.833, 0.624, 0.416, 0.312, 0.208 and 0.104 M (upward direction).

EPR measurements and DFT calculations

EPR measurements and deconvolution of the spectra.

X-band CW-EPR spectra were recorded with a BRUKER EleXsys E500 spectrometer (microwave frequency 9.4 GHz, microwave power 13 mW, modulation amplitude 5 G, modulation frequency 100 kHz). The concentration of measured samples in aqueous solutions were $c_{(CuL)}$ = 2.0 mM and 5% ligand excess for CB-15aneN$_5$ and 1.95 mM and 5% ligand excess for *p*NO$_2$Bn-CB-15aneN$_5$. The pH of the solutions was maintained by using HEPES (pH 7.2) and N-methyl-piperazine (pH 9.2) buffer solutions. Room temperature EPR spectra have been recorded in capillaries averaging 6 scans. Frozen solution EPR spectra were measured in quartz EPR tubes placed into Dewar containing liquid nitrogen at 77K. 0.2 mL samples have been introduced into the tubes and 0.05mL MeOH was added to avoid the crystallization of water. Before the simulation, all spectra have been corrected with the background spectrum of pure aqueous solution.

All CW-EPR spectra were simulated by the dedicated EPR software.[6] Room temperature spectra were described by the isotropic EPR parameters g_o and A_o^{Cu} copper hyperfine couplings, and the relaxation parameters α, β, γ which define the linewidths in the equation $\sigma_{MI} = \alpha + \beta M_I + \gamma M_I^2$, where M_I denotes the magnetic quantum number of copper nucleus. The anisotropic spectra were analysed by the anisotropic EPR parameters ($g_\perp$, $g_\parallel$, $A_\perp^{Cu}$, $A_\parallel^{Cu}$) and the orientation dependent linewidth parameters. Although nitrogen coupling would be expected in the spectra, this is not resolved because the value of the coupling constant is presumably less than the line width of the spectra. Since natural $CuCl_2$ was used for the measurements, the spectra were calculated as the sum of the spectra of ^{63}Cu and ^{65}Cu weighted by their natural abundances. The copper and nitrogen coupling constants and the relaxation parameters were obtained in field units (Gauss = 10^{-4} T).

DFT calculations and prediction of the EPR parameters

The geometries of the [Cu(CB-15aneN$_5$)]$^{2+}$ and [Cu(*p*NO$_2$Bn-CB-15aneN$_5$)]$^{2+}$ complexes were optimized through Gaussian 09 (Rev. E.01)[7] software at DFT level of theory using the hybrid Becke three-parameter B3P86 functional,[8] which is often used to predict the structure of transition metal species because of its high degree for accuracy.[9] The relativistic small-core ECPs SDD[10] (the Stuttgart-Dresden ECP) and LANL2DZ[11] with the corresponding valence basis sets were employed on the copper(II) and the triple-ζ *def2*-TZVP basis set for the main group elements. The solvent effect was taken into account adopting the Polarizable Continuum Model (PCM)[12] for water. Single point calculations were carried out for the ground state geometries which represented true minima on the potential energy surface, thus imaginary frequencies were not found. Cartesian coordinates of the copper(II) complexes were generated by EsiGen software[13] while Chimera (1.15)[14] was used to visualize the complexes.

The ORCA program (v4.0.1.2)[15] was used to calculate the ***g*** and ***A*** tensor for copper(II) coupling. The B3PW[8] hybrid functional, the long-range corrected CAM-B3LYP[16] functional, and the PBE0[17] employing PBE correlation functional were combined with the core-property basis set (CP(PPP)) for copper(II) and the EPR-II[18] for further elements in the calculations.

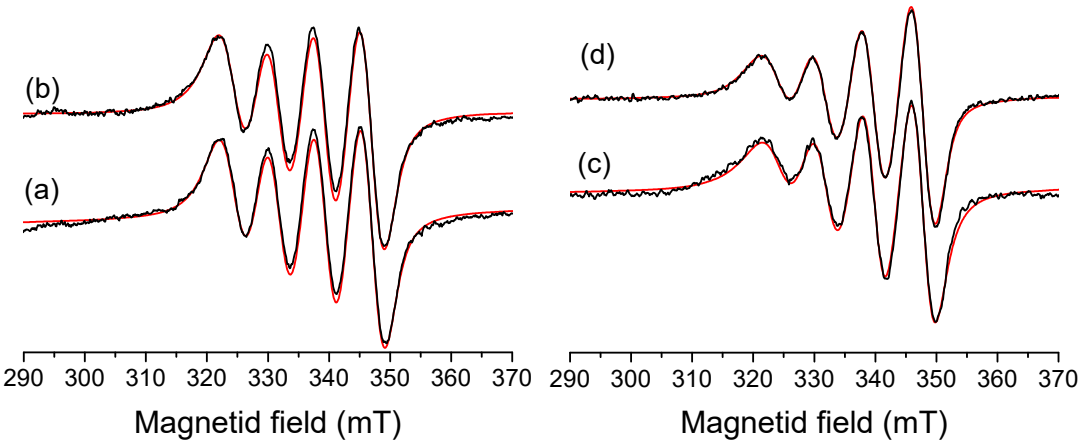

Figure S22. Experimental (black) and simulated (red) X-band CW-EPR spectra recorded at room temperature in aqueous solution of $[Cu(CB\text{-}15aneN_5)]^{2+}$ (a,b) and $[Cu(p NO_2Bn\text{-}CB\text{-}15aneN_5)]^{2+}$ (c,d) systems at pH 7.2 (a,c) and 9.2 (b,d).

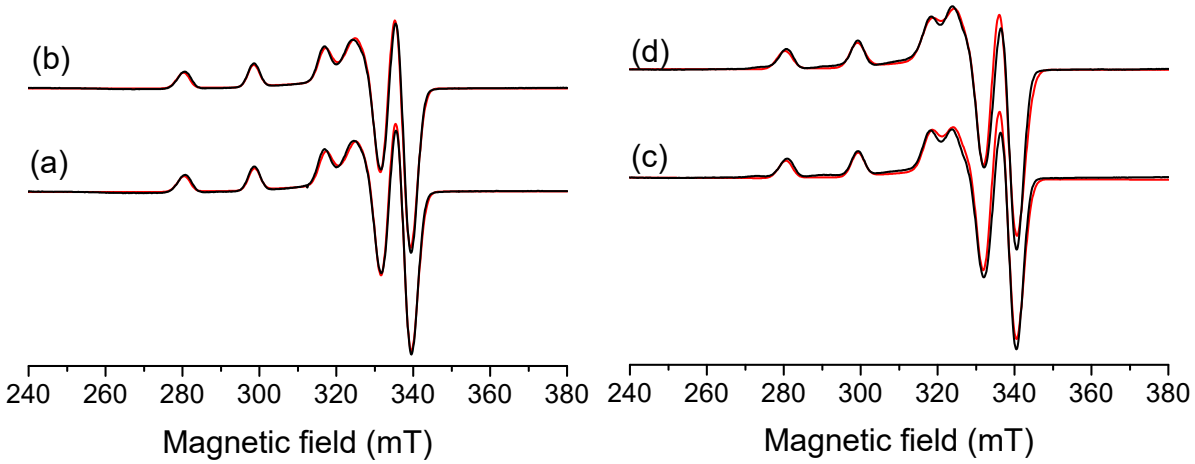

Figure S23. Experimental (black) and simulated (red) X-band CW-EPR spectra recorded at frozen solution (77 K) of $[Cu(CB\text{-}15aneN_5)]^{2+}$ (a,b) and $[Cu(p NO_2Bn\text{-}CB\text{-}15aneN_5)]^{2+}$ (c,d) systems at pH 7.2 (a,c) and 9.2 (b,d).

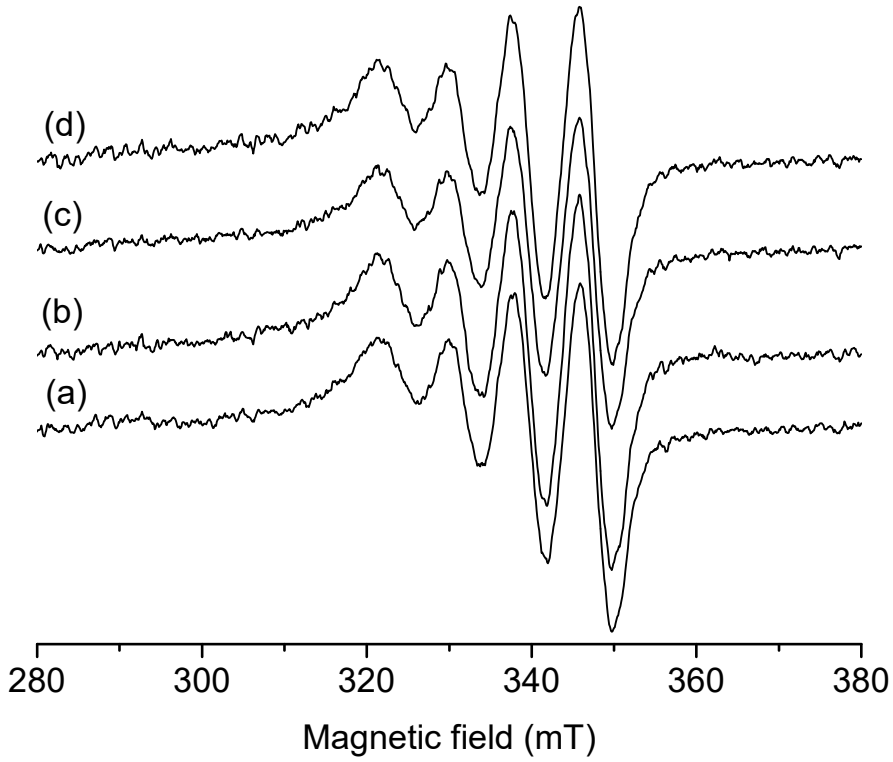

Figure S24. EPR spectra recorded at room temperature in aqueous solution of $[Cu(CB\text{-}15aneN_5)]^{2+}$ at (a) 1:0 , (b) 1:1, (c) 1:2 and (d) 1:4 complex : *N*-Methylimidazole ratios at pH 7.2. No spectral changes were detected proving that the axial coordination site is occupied by the CB-15aneN$_5$ ligand.

Table S3. Isotropic and anisotropic EPR parameters obtained by the simulation of room temperature and frozen solution spectra of $[Cu(CB\text{-}15aneN_5)]^{2+}$ and $[Cu(p NO_2Bn\text{-}CB\text{-}15aneN_5)]^{2+}$ complexes.

	Coordination mode	**Isotropic parameters[a]**		**Anisotropic parameters[b]**				**Calculated[c]**
		g_0	A_0 ($\times 10^4 cm^{-1}$)	$g_\perp$ or $g_{x,y}$	$g_\parallel$ or g_z	$A_\perp$ or $A_{x,y}$ ($\times 10^{-4} cm^{-1}$)	$A_\parallel$ or A_z ($\times 10^{-4} cm^{-1}$)	$g_{0,calc}$
$[Cu(CB\text{-}15aneN_5)]^{2+}$	5 N	2.096	71.7 (64.6)[d]	2.043	2.189	16.4	184.6 (177.5)[d]	2.0915
$[Cu(pNO_2Bn\text{-}CB\text{-}15aneN_5)]^{2+}$	5 N	2.094	75.2 (72.9)[d]	2.041	2.183	19.1	188.9 (188.6)[d]	2.088
[Cu(Cyclen)][e]	4 N			2.040, 2.055	2.197	16.9, 21.0	181.9	2.097
[Cu(DO4S)][f]	4 N			2.036	2.184	15.6	179.3	2.085

(a) The experimental error was ± 0.001 for g_0 and ± $1 \cdot 10^{-4}$ cm^{-1} for A_0. (b) The experimental error was ± 0.002 for $g_\perp$ and ± 0.001 for $g_\parallel$ and ± $1 \cdot 10^{-4}$ cm^{-1} for $A_\perp$ and $A_\parallel$. (c) Calculated by the equation g_0,calc = $(2g_\perp + g_\parallel)/3$ on the basis of anisotropic values. (d) Obtained by DFT calculations. (e) Data are taken from Ref.[19], (f) Data are taken from Ref.[20]

Table S4. Isotropic EPR parameters of the components obtained from the simulation of room temperature solution spectra of Cu(II)- CB-15aneN$_5$ or Cu(II)- *p*NO$_2$Bn-CB-15aneN$_5$

	g_0	A_0 (G)	α (G)	β (G)	γ (G)
Cu_{aq}^{2+}	2.1937	33.4	51	-1	0.1
$[Cu(CB\text{-}15aneN_5)]^{2+}$	2.0959	73.3	27	-4	0.96
$[Cu(pNO_2Bn\text{-}CB\text{-}15aneN_5)]^{2+}$	2.0941	76.9	32	-8	2.7

Table S5. Anisotropic EPR parameters of the components obtained from the simulation of frozen solution spectra (77K).

	g_x, g_y	g_z	A_x, A_y (G)	A_z(G)	α_x, α_y (G)	α_z (G)	β_x, β_y (G)	β_z (G)	γ_x, γ_y (G)	γ_z (G)
Cu_{aq}^{2+}	2.084	2.423	5.0	111.6	19.1	3.2	-17.7	-11.4	10.8	-4.7
$[Cu(CB\text{-}15aneN_5)]^{2+}$	2.043	2.189	17.2	180.7	20.4	12.9	1.4	8.2	-0.2	4.1
$[Cu(pNO_2Bn\text{-}CB\text{-}15aneN_5)]^{2+}$	2.042	2.182	20.9	185.1	21.6	14.3	0.0	9.9	0.0	4.50

Table S6. Cartesian Coordinates of the $[Cu(CB\text{-}15aneN_5)]^{2+}$ complex.

Sum of electronic and zero-point Energies (Eh)	-945.886725
Sum of electronic and thermal Energies (Eh)	-945.870584
Sum of electronic and enthalpy Energies (Eh)	-945.869639
Sum of electronic and thermal Free Energies (Eh)	-945.928299
Number of Imaginary Frequencies	0

Molecular Geometry in Cartesian Coordinates

C	3.084946	-0.382114	-0.329593
C	0.943398	2.713338	0.024932
C	1.640435	-2.388510	0.195380
C	-0.330479	2.623540	0.859208
C	0.559554	-2.196108	1.259339
H	3.924889	-0.748712	-0.920433
H	1.373371	-3.196290	-0.483015
H	0.716519	2.807733	-1.037581
H	3.333288	-0.523436	0.723302
H	1.525070	3.589546	0.323121
H	2.568621	-2.687686	0.683879
H	0.316875	-3.168890	1.701998
C	2.831924	1.093489	-0.593517
H	2.583709	1.266543	-1.641984
H	3.717187	1.684630	-0.348246
N	1.855480	-1.162230	-0.616983
H	1.857496	-1.414740	-1.598955
N	1.672894	1.458839	0.227262
H	1.932233	1.375359	1.207387
N	-0.633863	-1.530783	0.709829
N	-1.032292	1.320806	0.664013
C	-1.230327	0.570897	1.934081
H	-0.311853	0.672704	2.512337
H	-2.033494	1.018395	2.527984
C	-1.529950	-0.910979	1.706687
H	-2.555177	-1.042252	1.364301
H	-1.464258	-1.427682	2.667602
C	-2.266551	1.420472	-0.151302

H	-2.676376	2.429526	-0.090654
H	-3.016627	0.761607	0.283404
C	-2.027150	1.051182	-1.604934
H	-2.991351	1.022331	-2.123024
H	-1.416085	1.809392	-2.096471
N	-1.308125	-0.227562	-1.698955
C	-2.102587	-1.396790	-1.282264
H	-2.401801	-1.988977	-2.147658
H	-3.025673	-1.047829	-0.820098
C	-1.338838	-2.301741	-0.317851
H	-2.027440	-3.026454	0.129179
H	-0.598704	-2.869584	-0.878745
H	-0.996953	3.449757	0.615094
Cu	0.292775	0.071007	-0.244187
H	-0.972221	-0.354158	-2.644923
H	0.943087	-1.561301	2.060042
H	-0.079721	2.717728	1.916409

Table S7. Cartesian Coordinates of the $[Cu(p NO_2Bn\text{-}CB\text{-}15aneN_5)]^{2+}$ complex.

Sum of electronic and zero-point Energies (Eh)	-1382.621882
Sum of electronic and thermal Energies (Eh)	-1382.598502
Sum of electronic and enthalpy Energies (Eh)	-1382.597558
Sum of electronic and thermal Free Energies (Eh)	-1382.673964
Number of Imaginary Frequencies	0

Molecular Geometry in Cartesian Coordinates

C	-0.690021	2.694718	1.605468
C	-1.850335	2.087535	-1.952668
C	-1.010465	0.531077	2.908300
C	-2.838525	0.948721	-2.191470
C	-2.222651	-0.322886	2.535691
H	0.064671	3.262820	2.149715
H	-0.223535	-0.082846	3.342143
H	-0.865782	1.856383	-2.359900
H	-1.658512	2.911324	2.057911
H	-2.208008	2.997443	-2.440455
H	-1.305449	1.247431	3.675717
H	-2.486030	-0.970755	3.377434
C	-0.709971	3.084621	0.134084
H	0.252904	2.880115	-0.336275
H	-0.928011	4.148742	0.023472
N	-0.439631	1.235214	1.728709
H	0.564207	1.085874	1.713950
N	-1.731351	2.240835	-0.499432
H	-2.640899	2.499315	-0.121889
N	-1.988987	-1.114603	1.304410
N	-2.534503	-0.243345	-1.340330
C	-3.678214	-0.657511	-0.483264
H	-4.115100	0.249367	-0.065575
H	-4.454979	-1.146457	-1.078079
C	-3.232855	-1.585337	0.644084
H	-3.052767	-2.589693	0.265422
H	-4.041747	-1.675660	1.371692
C	-1.947428	-1.380362	-2.084464
H	-2.267351	-1.347146	-3.126893
H	-2.351771	-2.303130	-1.677068
C	-0.431940	-1.383167	-2.055772
H	-0.068277	-2.242835	-2.627821

H	-0.090464	-0.486815	-2.564279
N	0.126188	-1.385933	-0.690123
C	-0.311194	-2.536157	0.125891
H	0.534188	-3.192508	0.336888
H	-0.993608	-3.129375	-0.477817
C	-0.980290	-2.170022	1.451729
H	-1.423585	-3.074619	1.879421
H	-0.238072	-1.820087	2.165503
C	1.470794	-0.993610	-0.551414
C	2.165761	-1.267220	0.638473
C	2.156986	-0.300075	-1.561164
C	3.466717	-0.852534	0.821790
H	1.695532	-1.806935	1.445392
C	3.457591	0.117504	-1.380453
H	1.696917	-0.082892	-2.511066
C	4.107949	-0.155232	-0.188390
H	3.984964	-1.068027	1.744669
H	3.973186	0.648514	-2.167262
N	5.472612	0.286429	0.000622
O	6.011629	0.898777	-0.907599
O	6.020959	0.027439	1.060212
H	-2.841931	0.666793	-3.243539
Cu	-1.300185	0.388181	0.124470
H	-3.081725	0.321111	2.339713
H	-3.846057	1.286996	-1.947342

Table S8. Calculated and experimental A_z, g_z and g_0 values for the $[Cu(CB\text{-}15aneN_5)]^{2+}$ and $[Cu(p NO_2Bn\text{-}CB\text{-}15aneN_5)]^{2+}$ complexes.[a]

	g_z	g_0	A_z (MHz)	A_z / 10^{-4} cm^{-1}
		$[Cu(CB\text{-}15aneN_5)]^{2+}$		
Experimental	2.189	2.096	553.4	184.6
B3PW	2.135 (-2.5)	2.075 (-1.0)	532.0	177.5 (-3.9)
PBE0	2.151 (-1.7)	2.083 (-0.6)	554.6	185.0 (0.2)
CAM-B3LYP	2.147 (-4.2)	2.082 (-1.4)	547.3	182.6 (-1.1)
		$[Cu(p NO_2Bn\text{-}CB\text{-}15aneN_5)]^{2+}$		
Experimental	2.183	2.088	566.3	188.9
B3PW	2.127 (-2.6)	2.069 (-0.9)	565.4	188.6 (-0.2)
PBE0	2.142 (-1.9)	2.077 (-0.5)	591.1	197.2 (4.4)
CAM-B3LYP	2.139 (-2.0)	2.076 (-0.6)	585.2	195.2 (3.3)

[a] Percent deviations are shown in parenthesis.

Kinetic measurements

The rate of the formation of the two Cu(II) complexes was studied at 25 °C and 0.15 M NaCl ionic strength in the presence of 10 times ligand excess to ensure pseudo-first order conditions. The absorbance change was monitored at 285 nm (CB-15aneN_5) and 565 nm (*p*NO_2Bn-CB-15aneN_5) with a Cary 100 Bio UV-vis spectrophotometer. The ligand concentrations in the reactions were 0.2 mM for CB-15aneN_5 and 2 mM for *p*NO_2Bn-CB-15aneN_5, respectively. The reactions were carried out in the pH range 2.0-3.8 for the Cu(II)-CB-15aneN_5 and 3.3–5.0 for the Cu(II)-*p*NO_2Bn-CB-15aneN_5 systems using buffers such as chloroacetic acid (pK_a = 2.9) and DMP (1,4-dimethylpiperazine, pK_a = 4.2) in 50 mM concentration, respectively.

The inertness of the complexes was investigated in 5.0 M HCl at 50 °C. The concentrations of the complexes were 0.2 mM ([Cu(CB-15aneN_5)]$^{2+}$) and 2 mM ([Cu(*p*NO_2Bn-CB-15aneN_5)]$^{2+}$) and the dissociation reactions were followed at 285 and 565 nm, respectively.

Labeling experiments

All chemicals (hydrochloric acid, ammonium acetate, water) used for labeling were ultrapure grade from VWR and Carl-Roth GmbH. TK400 and CU extraction resins were purchased from Triskem and loaded to 1ml empty syringes with PE frits.

^{61}Cu was produced from natural zinc powder (Sigma Aldrich, 99.999%) by pressing 50 mg powder to a pellet and irradiating with 15.5 MeV protons (10 min., 50 μA) in a GE PETtrace cyclotron. The irradiated target material was dissolved from its holder with 5 ml 7 M HCl, and passed through a small (15 x 9 mm) TK400 resin cartridge to remove the formed gallium isotopes. The solution was mixed with 10 ml 7 M ammonium formate to increase the pH above 2 and loaded to a CU resin column (10 x 9 mm). After washing with 20 ml water, the trapped activity was eluted with 0.5 ml 2 M HCl.

Labeling experiments were performed in 1 ml Eppendorf tubes at room temperature. 10 μl ^{61}Cu solution was mixed with 80 μl 1 M pH = 6 ammonium acetate buffer and 10 μl chelator solution. Labeling reactions were followed with radio-TLC using ITLC-SG (Agilent) strips, eluted with pH = 5.5 0.5 M citrate buffer and scanned in a MiniGita TLC scanner (Raytest).

Optimal pH for labeling was determined in various buffers (acetate from 4.5 to 6.5, HEPES for 7 and borate for 8.7) at room temperature and 2.5 μM chelator concentration.

Stability of the labelled chelator was investigated in 5 mM DTPA solution and mouse plasma at pH = 6 for DTPA and 7.4 for plasma and at room temperature. The change of radiochemical purity was followed with radio-TLC.

The data reproducibility was within 5% of error.

References

1 C. J. Anderson, T. J. Wadas, E. H. Wong and G. R. Weisman, Cross-bridged macrocyclic chelators for stable complexation of copper radionuclides for PET imaging, *Q J Nucl Med Mol Imaging*, 2008, **52**, 185–192.

2 R. Ferdani, D. J. Stigers, A. L. Fiamengo, L. Wei, B. T. Y. Li, J. A. Golen, A. L. Rheingold, G. R. Weisman, E. H. Wong and C. J. Anderson, Synthesis, Cu(ii) complexation, ^{64} Cu-labeling and biological evaluation of cross-bridged cyclam chelators with phosphonate pendant arms, *Dalton Trans.*, 2012, **41**, 1938–1950.

3 A. D. Shircliff, B. P. Burke, D. J. Davilla, G. E. Burgess, F. A. Okorocha, A. Shrestha, E. M. A. Allbritton, P. T. Nguyen, R. L. Lamar, D. G. Jones, M.-J. Gorbet, M. B. Allen, J. I. Eze, A. T. Fernandez, D. Ramirez, S. J. Archibald, T. J. Prior, J. A. Krause, A. G. Oliver and T. J. Hubin, An ethylene cross-bridged pentaazamacrocycle and its Cu $^{2+}$ complex: constrained ligand topology and excellent kinetic stability, *Chem. Commun.*, 2020, **56**, 7519–7522.

4 H. M. Irving, M. G. Miles and L. D. Pettit, A study of some problems in determining the stoicheiometric proton dissociation constants of complexes by potentiometric titrations using a glass electrode, *Analytica Chimica Acta*, 1967, **38**, 475–488.

5 L. Zekany and I. Nagypal, in *Computational Methods for the Determination of Formation Constants*, ed. D. J. Leggett, Springer US, Boston, MA, 1985, pp. 291–353.

6 A. Rockenbauer and L. Korecz, Automatic computer simulations of ESR spectra, *Appl. Magn. Reson.*, 1996, **10**, 29–43.

7 Frisch, M. J.; Trucks, G. W.; Schlegel, H. B.; Scuseria, G. E.; Robb, M. A.; Cheeseman, J. R.; Scalmani, G.; Barone, V.; Mennucci, B.; Petersson, G. A.; Nakatsuji, H.; Caricato, M.; Li, X.; Hratchian, H. P.; Izmaylov, A. F.; Bloino, J.; Zheng, G.; Sonnenberg, J. L.; Hada, M.; Ehara, M.; Toyota, K.; Fukuda, R.; Hasegawa, J.; Ishida, M.; Nakajima, T.; Honda, Y.; Kitao, O.; Nakai, H.; Vreven, T.; Montgomery Jr., J. A.; Peralta, J. E.; Ogliaro, F.; Bearpark, M. J.; Heyd, J.; Brothers, E. N.; Kudin, K. N.; Staroverov, V. N.; Kobayashi, R.; Normand, J.; Raghavachari, K.; Rendell, A. P.; Burant, J. C.; Iyengar, S. S.; Tomasi, J.; Cossi, M.; Rega, N.; Millam, N. J.; Klene, M.; Knox, J. E.; Cross, J. B.; Bakken, V.; Adamo, C.; Jaramillo, J.; Gomperts, R.; Stratmann, R. E.; Yazyev, O.; Austin, A. J.; Cammi, R.; Pomelli, C.; Ochterski, J. W.; Martin, R. L.; Morokuma, K.; Zakrzewski, V. G.; Voth, G. A.; Salvador, P.; Dannenberg, J. J.; Dapprich, S.; Daniels, A. D.; Farkas, Ö.; Foresman, J. B.; Ortiz, J. V.; Cioslowski, J.; Fox, D. J. Gaussian 09, Gaussian, Inc.: Wallingford, CT, USA, 2009., .

8 A. D. Becke, Density-functional thermochemistry. III. The role of exact exchange, *The Journal of Chemical Physics*, 1993, **98**, 5648–5652.

9 M. Bühl and H. Kabrede, Geometries of Transition-Metal Complexes from Density-Functional Theory, *J. Chem. Theory Comput.*, 2006, **2**, 1282–1290.

10 M. Dolg, U. Wedig, H. Stoll and H. Preuss, Energy-adjusted *a b i n i t i o* pseudopotentials for the first row transition elements, *The Journal of Chemical Physics*, 1987, **86**, 866–872.

11 P. J. Hay and W. R. Wadt, *Ab initio* effective core potentials for molecular calculations. Potentials for K to Au including the outermost core orbitals, *The Journal of Chemical Physics*, 1985, **82**, 299–310.
12 J. Tomasi, B. Mennucci and R. Cammi, Quantum Mechanical Continuum Solvation Models, *Chem. Rev.*, 2005, **105**, 2999–3094.
13 J. Rodríguez-Guerra Pedregal, P. Gómez-Orellana and J.-D. Maréchal, ESIgen: Electronic Supporting Information Generator for Computational Chemistry Publications, *J. Chem. Inf. Model.*, 2018, **58**, 561–564.
14 E. F. Pettersen, T. D. Goddard, C. C. Huang, G. S. Couch, D. M. Greenblatt, E. C. Meng and T. E. Ferrin, UCSF Chimera?A visualization system for exploratory research and analysis, *J. Comput. Chem.*, 2004, **25**, 1605–1612.
15 F. Neese, The ORCA program system, *WIREs Comput Mol Sci*, 2012, **2**, 73–78.
16 T. Yanai, D. P. Tew and N. C. Handy, A new hybrid exchange–correlation functional using the Coulomb-attenuating method (CAM-B3LYP), *Chemical Physics Letters*, 2004, **393**, 51–57.
17 J. P. Perdew, K. Burke and M. Ernzerhof, Generalized Gradient Approximation Made Simple, *Phys. Rev. Lett.*, 1996, **77**, 3865–3868.
18 D. P. Chong, *Recent Advances in Density Functional Methods: (Part I)*, WORLD SCIENTIFIC, 1995, vol. 1.
19 S. Lacerda, M. P. Campello, I. C. Santos, I. Santos and R. Delgado, Study of the cyclen derivative 2-[1,4,7,10-tetraazacyclododecan-1-yl]-ethanethiol and its complexation behaviour towards d-transition metal ions, *Polyhedron*, 2007, **26**, 3763–3773.
20 M. Tosato, M. Dalla Tiezza, N. V. May, A. A. Isse, S. Nardella, L. Orian, M. Verona, C. Vaccarin, A. Alker, H. Mäcke, P. Pastore and V. Di Marco, Copper Coordination Chemistry of Sulfur Pendant Cyclen Derivatives: An Attempt to Hinder the Reductive-Induced Demetalation in $^{64/67}$ Cu Radiopharmaceuticals, *Inorg. Chem.*, 2021, **60**, 11530–11547.